Xu et al. *Zool. Res.* 2024, 45(2): 381−397
https://doi.org/10.24272/j.issn.2095-8137.2023.293

ZR | Zoological Research

Article Open Access

Identification and effective regulation of *scarb1* gene involved in pigmentation change in autotetraploid *Carassius auratus*

Xi-Dan Xu[1,4], Yue Zhou[1], Chong-Qing Wang[1], Xu Huang[1], Kun Zhang[1], Xiao-Wei Xu[1], Li-Wen He[1], Xin-Yue Zhang[1], Xin-Zhu Fu[1], Ming Ma[4], Qin-Bo Qin[1,2,3,*], Shao-Jun Liu[1,*]

[1] *State Key Laboratory of Developmental Biology of Freshwater Fish*, *Engineering Research Center of Polyploid Fish Reproduction and Breeding of the State Education Ministry*, *College of Life Sciences*, *Hunan Normal University*, *Changsha*, *Hunan* 410081, *China*
[2] *Nansha-South China Agricultural University Fishery Research Institute*, *Guangzhou*, *Guangdong* 511458, *China*
[3] *Hunan Yuelu Mountain Science and Technology Co. Ltd. for Aquatic Breeding*, *Changsha*, *Hunan* 410081, *China*
[4] *College of Chemistry and Chemical Engineering*, *Hunan Normal University*, *Changsha*, *Hunan* 410081, *China*

ABSTRACT

The autotetraploid *Carassius auratus* (4nRR, 4*n*=200, RRRR) is derived from whole-genome duplication of *Carassius auratus* red var. (RCC, 2*n*=100, RR). In the current study, we demonstrated that chromatophores and pigment changes directly caused the coloration and variation of 4nRR skin (red in RCC, brownish-yellow in 4nRR). To further explore the molecular mechanisms underlying coloration formation and variation in 4nRR, we performed transcriptome profiling and molecular functional verification in RCC and 4nRR. Results revealed that *scarb1*, associated with carotenoid metabolism, underwent significant down-regulation in 4nRR. Efficient editing of this candidate pigment gene provided clear evidence of its significant role in RCC coloration. Subsequently, we identified four divergent *scarb1* homeologs in 4nRR: two original *scarb1* homeologs from RCC and two duplicated ones. Notably, three of these homeologs possessed two highly conserved alleles, exhibiting biased and allele-specific expression in the skin. Remarkably, after precise editing of both the original and duplicated *scarb1* homeologs and/or alleles, 4nRR individuals, whether singly or multiply mutated, displayed a transition from brownish-yellow skin to a cyan-gray phenotype. Concurrently, the proportional areas of the cyan-gray regions displayed a gene-dose correlation. These findings illustrate the subfunctionalization of duplicated *scarb1*, with all *scarb1* genes synergistically and equally contributing to the pigmentation of 4nRR. This is the first report concerning the functional differentiation of duplicated homeologs in an autopolyploid fish, substantially enriching our understanding of coloration formation and change within this group of organisms.

Keywords: Autopolyploidization; Coloration change; *scarb1*; Functional differentiation; Genetic changes

INTRODUCTION

Polyploidization is considered a driving force of both evolution and biodiversity (Van De Peer et al., 2017). Polyploid organisms contain multiple sets of genetic material and exhibit genome restructuring and wide reorganization of gene expression after genomic merging and doubling (Levy & Feldman, 2004). This process can lead to the emergence of trait innovation that aids in ecological adaptation and survival demands of the organisms (Song et al., 2012a). Polyploid breeding, which can result in whole-genome duplication (WGD) accompanied by alterations and innovations in biological traits, holds considerable value for the acquisition of superior traits. This approach has yielded remarkable economic and social benefits, with wide application in the improvement of various crops, such as cotton, wheat, and *Arabidopsis* (Awan et al., 2022; Chen et al., 2020; Corneillie et al., 2019), as well as in the enhancement of fish genetic resources (Hu et al., 2020; Wang et al., 2020b). In this study, autotetraploid *Carassius auratus* (4nRR, 4*n*=200), derived from the distant hybridization of *Carassius auratus* red var. (RCC, 2*n*=100) (♀) × *Megalobrama amblycephala* (BSB, 2*n*=48) (♂) (Qin et al., 2014), exhibited stable genetic traits

Received: 24 November 2023; Accepted: 25 December 2023; Online: 26 December 2023
Foundation items: This work was supported by the National Natural Science Foundation of China (32172972, U19A2040), Science and Technology Innovation Program of Hunan Province (2021RC4028), Earmarked Fund for China Agriculture Research System (CARS-45), Hunan Provincial Science and Technology Department (2019RS5001), Special Funds for Construction of Innovative Provinces in Hunan Province (2021NK1010), Special Science Found of Nansha-South China Agricultural University Fishery Research Institute, Guangzhou (NSYYKY202305, NSYYKY202306), and Aid Program for Science and Technology Innovative Research Team in Higher Educational Institutions of Hunan Province.
*Corresponding authors, E-mail: qqb@hunnu.edu.cn; lsj@hunnu.edu.cn

and biological characteristics, and maintained autotetraploid line formation (F_1–F_{18}). Previous studies have demonstrated that 4nRR harbors four sets of chromosomes derived from RCC, a consequence of WGD. Notably, the most prominent distinction between these variants is their pigmentation: diploid RCC is characterized by a red coloration, accompanied by temporal change in body color, whereas 4nRR maintains a consistent brownish-yellow coloration. To date, research on genetic and phenotypic changes after autopolyploidization has predominantly focused on plants, with few studies reported on fish. The autotetraploid *Carassius auratus*, therefore, provides an exemplary model for exploring the genetic basis of color variation following autopolyploidization.

Coloration and pigmentation patterns are prominent phenotypic features in vertebrates, evolving through selection and adaptation and displaying a wide functional spectrum in life history and behavior such as camouflage, thermoregulation, and selective mating (Hubbard et al., 2010; Parichy, 2003). Compared with mammals that rely solely on melanocytes, the distinctive and captivating color and pigment patterns in fish are primarily generated through the combined and organized distribution of different chromatophores widely scattered throughout the hypodermis, epidermis, scales, and fins (Bagnara & Matsumoto, 2006; Fujii, 1993). While the genetic basis of the diversity and complexity of pigment phenotypes in fish, particularly teleosts, remains elusive, the functional diversification of pigment genes following gene duplication during fish-specific genome duplication (FSGD) events is considered a potential contributing factor (Braasch et al., 2007, 2009; Meyer & Van De Peer, 2005). Polyploidy has occurred repeatedly in certain taxonomic fish orders. Common carp (*Cyprinus carpio*) and goldfish, for instance, have undergone additional allotetraploid events and developed into different strains exhibiting diverse morphological and color variations (Chen et al., 2019; Xu et al., 2014, 2019). However, the mechanisms underlying fish coloration formation and differentiation, particularly in hybrid fish, are exceedingly complex and do not entirely align with Mendelian inheritance (David et al., 2004; Li et al., 2023; Shirak et al., 2000). Noticeably, marked non-Mendelian changes in coloration have been observed in the newly synthesized 4nRR compared to RCC, BSB, and their allotetraploid hybrids (F_1, 4*n*=148, RRBB, brownish-yellow coloration). At present, the molecular genetic mechanisms underpinning coloration variation in 4nRR remain less well understood.

Currently, the significance and implications of autotetraploidization on genetic and epigenetic changes in 4nRR genomes have been supported from whole-genome re-sequencing, full-length transcriptomes, amplified fragment length polymorphism (AFLP), and methylation-sensitive amplification polymorphism (MSAP) analyses (Wang et al., 2020a, 2021b). However, despite advances in our understanding of genomic and transcriptomic changes in autotetraploids, the molecular and genetic basis of pigmentation variation remains incompletely understood. Recently, hub gene editing-based molecular breeding technologies have been applied to some diploid and polyploid aquaculture species to improve genetic resources and generate desirable traits (Yu et al., 2021, 2022). Hence, proposed candidate pigment gene editing-based molecular breeding that allows the appearance of novel or tailored traits may be conducive to revealing the genetic basis of pigmentation and coloration variation following autopolyploidization. In the present study, we explored the skin chromatophores and carotenoids in both RCC and 4nRR and identified a key pigment gene involved in carotenoid-based pigmentation of the skin. Subsequently, we edited the proposed candidate pigment gene to determine the regulatory and functional mechanisms underlying coloration change. To the best of our knowledge, this is the first report on coloration variation of an autotetraploid fish using gene knockout. This study not only advances our understanding of the molecular mechanisms underlying pigmentation and coloration variations in 4nRR but also provides insights into the molecular mechanisms underlying phenotypic variations in autopolyploid animals.

MATERIALS AND METHODS

Experimental fish and samples

The RCC and 4nRR fish were cultivated at the State Key Laboratory of Developmental Biology of Freshwater Fish, Hunan Normal University, China. All experimental fish were maintained in an open pool (0.067 ha) under optimal pH (7.0–8.5), water temperature (22–24°C), and dissolved oxygen (5.0–8.0 mg/L) conditions and provided with suitable forage. The *scarb1* gene sequence was derived using cDNA and DNA from intestinal samples as templates. In wild-type (WT) specimens, the expression patterns of *scarb1* were analyzed in the red skin of adult RCC and in the brownish-yellow skin of adult 4nRR, specifically the upper region above the lateral line. In the case of single *scarb1* homeologs knockout mutants, a shift to yellow skin coloration was observed in RCC (abbreviated as SK-Y), while 4nRR retained its brownish-yellow coloration (SK-BY). Quantitative analysis of the unmodified *scarb1* homeolog was carried out on the yellow skin region of RCC (SK-Y), along with the brownish-yellow (SK-BY) and cyan-gray skin regions (SK-CG) in 4nRR, respectively. In individuals mutated with simultaneous disruption of *scarb1* homeologs, the skin on RCC was categorized into three regions based on coloration changes and pigment cell composition: orange-yellow region (with xanthophores and erythrophores, M-OY), shallow yellow region (with xanthophores, M-SY), and white region (non-pigment, M-W). Given the subtle boundary distinction between the shallow yellow and white regions, we also conducted mixed sampling of these two areas (M-S), using M-OY and M-S as experimental materials for subsequent quantitative experiments. For the 4nRR mutants, the skin regions were classified based on similar pigmentation distribution into a brownish-yellow region (with xanthophores and melanophores, M-BY) and a cyan-gray region (with melanophores, M-CG). All fish tissues were surgically collected under anesthesia using 100 mg/L MS-222 (Sigma-Aldrich, USA).

Identification of carotenoid differences in RCC and 4nRR

Three biological replicates were used for both the 12-month-old WT RCC and 4nRR fish, generated from the March 2020 reproductive season. A total of 800 mg of skin tissue was collected from each fish, with 500 mg allocated to assess total carotenoid content and 300 mg used to identify carotenoid pigments and quantify monomeric content. Total carotenoids were initially extracted using a combination of petroleum ether and ethanol. The concentrations of carotenoids were then

measured through absorbance spectrophotometry at an excitation wavelength of 450 nm (Clotfelter et al., 2007; Steffen & McGraw, 2007). Carotenoids were identified utilizing ultra-performance liquid chromatography (UPLC) as detailed in Meléndez-Martínez et al. (2010), then compared to known standards, including zeaxanthin, β-cryptoxanthin, xanthophyll (lutein), beta-carotene, α-carotene, lycopene, capsanthin, violaxanthin, neoxanthin, and astaxanthin (Sigma, Germany). The skin extracts were analyzed using a UPLC system (UPLC, U3000; Thermo Fisher Scientific, USA). Data were acquired on the U3000 UPLC (Thermo Fisher Scientific, USA) and processed using Chromeleon v7.2 CDS software (Thermo Fisher Scientific, USA).

Comparative analysis of skin transcriptomes and identification of candidate carotenoid-based genes in RCC and 4nRR

Three biological replicates were used for RCC and 4nRR skin transcriptomic analysis, sourced from the same individuals analyzed for carotenoid composition. Total extracted RNA concentration and quality were assessed using a NanoDrop-2000 spectrophotometer (Thermo Scientific, USA) and agarose (1.0%) gel electrophoresis, respectively. The cDNA was synthesized from high-quality RNA of each biological replicate. Six paired-end libraries (three for RCC and three for 4nRR) were constructed using a TruSeq^{TM} RNA Library Prep Kit (Illumina, USA), with subsequent end-repair, 3-end adenylation, adapter ligation, and enrichment. Clean data wereassessedusingFastQC(v0.11.9,http://www.bioinformatics.babraham.ac.uk/projects/fastqc/) and aligned to the 4nRR reference sequence (unpublished data) using STAR software. Quantification and normalization of transcript levels of genes were performed using Stringtie (v1.3.4d) and the Deseq2 R package (v1.26.0). Gene Ontology (GO) and Kyoto Encyclopedia of Genes and Genomes (KEGG) enrichment analyses of differentially expressed genes (DEGs) were implemented using the clusterProfiler R package (v3.14.0). Hub genes related to the coloration variation spectrum from yellow to red were identified in the RCC and 4nRR groups and verified by real-time RT-PCR (RT-qPCR).

Histological observation of pigment cells in skin

The combination and distribution of different pigment cell types contribute to the pigmentation and coloration patterns observed in fish. We identified chromatophore differences between the skins of RCC and 4nRR, as well as between the skins of WT and mutant individuals, using frozen sections and transmission electron microscopy (TEM). To identify the composition of skin pigment cells by light microscopy, fresh skin was immediately fixed in 4% paraformaldehyde for 12 h, embedded in OCT-freezing medium, and rapidly frozen in liquid nitrogen. The frozen tissue was subsequently cryosectioned to a thickness of 5 μm, with image acquired with a Leica DM2500 microscope (Leica, Germany). To examine the ultra-microscopic structure of skin pigment cells, skin samples were fixed in 2.5% glutaraldehyde at 4℃ for 12 h, treated with 2% OsO4 for 2 h, and washed with phosphate-buffered saline (PBS). After dehydration through an ethanol series, the specimens were embedded in epoxy resin, sectioned, stained with uranyl acetate for 2 h or overnight, coverslipped, then imaged using the Hitachi TEM system (JEM-1230, Japan) (Zhang et al., 2017). The skin samples were obtained at 4℃ and sampled with a portion of muscle tissue.

Cloning, sequence analysis, and RT-qPCR

Total RNA from all samples was extracted according to the TRIzol protocols (Thermo Scientific, USA), and the determination of RNA quality and concentration was the same as the method used for RNA in the skin transcriptomes. The cDNA was synthesized using a SMARTerTM PCR cDNA Synthesis Kit (Clontech, USA) based on the manufacturer's instructions. The cDNA and DNA amplification primers designed based on the genome sequences of RCC (ASM336829v1) and 4nRR (unpublished) are listed in Supplementary Table S1. The PCR products amplified by the primers were purified and cloned into DH5α competent cells to obtain the specific sequences of *scarb1* homeologs in RCC and 4nRR. Multiple amino acid sequence alignment and phylogenetic analysis were executed using DNAMAN (v7.0) and Molecular Evolutionary Genetics Analysis (MEGA 7), respectively (Kumar et al., 2016). All amino acid sequences used in this study were obtained from GenBank (http://www.ncbi.nlm.nih.gov/).

The RT-qPCR procedure was conducted as described by Wang et al. (2021a). All samples were performed in triplicate. The specific RT-qPCR primers for each gene are listed in Supplementary Table S1, with *β-actin* and *18S* selected as the optimal reference genes according to our previous study (Du et al., 2021; Wang et al., 2021a). The expression results were calculated using the $2^{-\Delta\Delta Ct}$ method (Livak, 2001), with the expression levels of the housekeeping genes acquired using geometric mean expression of *β-actin* and *18S*. Statistical analysis was performed using one-way analysis of variance (ANOVA). As divergent *scarb1* homeologs exhibited differences in their nucleotide sequences, differences in expression among the *scarb1* homeologs were analyzed using four unique pairs of primers designed to amplify *scarb1a*, *scarb1b*, *scarb1c*, and *scarb1d*, respectively, according to the different coding sequence (CDS) regions of the homeologs. Specific RT-qPCR amplification of the primers was then determined by clone sequencing. Subsequently, due to the extremely high identities of two alleles in the *scarb1* homeologs, the expression differences between two alleles of each *scarb1* homeolog were determined and RT-qPCR products amplified from the skin (n=3) were purified and cloned. In total, 30–36 clones of each sample were sequenced and classified according to the specific single nucleotide polymorphisms (SNPs) between the two alleles. The expression level was calculated based on the average ratio of sequencing clone numbers.

Generation of *scarb1*-mutated RCC and 4nRR by CRISPR/Cas9

Both *scarb1*-mutated RCC and 4nRR were generated using CRISPR/Cas9 technology. The single guide RNA (sgRNA) target site was chosen on the second exon to completely disrupt gene function, designed using the target online design program (http://crispr.mit.edu/,http://zifit.partners.org/ZiFiT/CSquare9Nuclease.aspx) (Supplementary Table S2). All sgRNAs (two for *scarb1a*, two for *scarb1b*, three for *scarb1c*, and three for *scarb1d*) were transcribed following the manufacturer's protocols using the RiboMAXTM Large Scale RNA Production System-T7 (Pomega, USA). The nls-Cas9-nls protein used was obtained from the NEB Company (USA). Agarose gel electrophoresis was applied to identify all qualified sgRNAs, appearing as a bright single band (slightly above 100 bp), which were then stored at −80°C until further use.

Analysis of egg characteristics revealed that the average egg diameter of 4nRR fish was significantly larger than that of RCC, with a difference of up to 0.5 mm (Wang et al., 2019). Additionally, 4nRR possessed an extra set of chromosomes compared to RCC. Mixtures of *in vitro*-synthesized sgRNAs (150–200 ng/μL) obtained within one month and Cas9 protein (20 pmol/μL) were co-injected into one-cell stage embryos. The injection volume for the RCC embryos was one-eighth of the volume of the zygote, while was twice that of RCC for 4nRR. We identified two divergent *scarb1* homeologs (*scarb1a* and *scarb1b*) in RCC and four divergent *scarb1* homeologs (*scarb1a*, *scarb1b*, *scarb1c*, and *scarb1d*) in 4nRR. Except for *scarb1d*, for which only one gene was identified, each *scarb1* homeolog contained two alleles with high nucleotide and amino acid identities. Biallelic mutation of each *scarb1* homeolog was implemented by the same specificity sgRNAs. Thus, we performed single-homeolog and multi-homeolog knockout, respectively, to further explore the association of homologous genes and the function of *scarb1* homeologs. All F_0 individuals with mutations in *scarb1a-A*/*scarb1a-B*, *scarb1b-A*/*scarb1b-B*, *scarb1c-A*/*scarb1c-B*, or *scarb1d* were produced by disrupting the respective genes. Likewise, F_0 individuals with mutations in both *scarb1a* and *scarb1b* in RCC or *scarb1a*, *scarb1b*, *scarb1c*, and *scarb1d* in 4nRR were generated. Consequently, three mosaic mutants in RCC and five mosaic mutants in 4nRR were obtained. As the hatching rate of 4nRR embryos is lower than that of RCC, all injected embryos were developed in purified water at 22℃. Once they began to swim horizontally, they were moved to outdoor rearing for observation. All mutants were maintained in the same open-air environment with sufficient sunlight.

Classification and observation of mutants

At 24 h after microinjection, DNA was extracted from 30 injected embryos to test editing efficiency. We conducted PCR-specific amplification and sequence analysis of each target region of the *scarb1* homeologs. Preliminary investigations of the 30 injected samples showed that 27 displayed overlapping peaks in target genes. These samples were sub-cloned into the pM18-T vector (Takara, Japan), and at least 30 colonies were randomly selected from each sample and sequenced. Twenty out of 27 individuals were *scarb1*-modified with high mutation rate (rate of mutant clones over 80%). None of the embryos displayed a uniformly mutated *scarb1* sequence. Additionally, mutant sequences could not be aligned to the WT sequence, indicating the potential presence of cells with various genotypes in the fish. Thus, we applied similar PCR-specific amplification and sequence analysis to adult mosaic mutants with varied phenotypes. Blood genomic DNA was used as the template for further genotyping. Phenotypic traits of all mosaic fish were imaged on a white background.

RESULTS

Histological observation and carotenoid pigment determination in RCC and 4nRR skin

Chromatophores, cells that contain pigment and reflect light, play a crucial role in the development of skin color, and can be subdivided into different pigment cell types based on the color they impart. Given the distinct coloration and pigmentation observed between red RCC and brownish-yellow 4nRR, we first investigated their skin pigment cells. Examination of cryosections revealed the presence of melanophores and xanthophores in 4nRR (Figure 1D), in contrast to the exclusive presence of erythrophores in RCC (Figure 1A). Further TEM analysis confirmed the presence of erythrophores and iridophores in RCC (Figure 1B, C), as well as the coexistence of melanophores, xanthophores, and iridophores in 4nRR (Figure 1E, F). These observations suggest that autotetraploidization significantly altered the composition of pigment cells, endowing 4nRR with higher chromatophore diversity compared to its diploid parent.

Yellow, orange, and red colors in fish are attributed to carotenoids stored in xanthophores or erythrophores. Xanthophores and erythrophores typically include a mixture of different carotenoids, which are directly deposited within the cells. Given the differences in xanthophores and erythrophores between RCC and 4nRR, we subsequently determined total carotenoid content and carotenoid pigments in the skins of both fish. Pigment analysis revealed that the average total carotenoid content was significantly higher in RCC skins than in 4nRR skins (P<0.01), and the red skin samples (average 0.98926 mg/g) had, on average, two times more carotenoids than the brownish-yellow skin (average 0.47309 mg/g) (Figure 1G). Moreover, based on comparison with available carotenoid standards, three types of carotenoids (violaxanthin, lutein, and zeaxanthin) were identified by HPLC in both RCC and 4nRR, while other carotenoids, including neoxanthin, astaxanthin, and b-carotene, were only found in RCC (Figure 1H). Of note, lutein, as the most abundant carotenoid pigment detected in both fish, was significantly down-regulated in 4nRR (average 200.4535×0.01 ng/mg) compared to RCC (average 527.5251×0.01 ng/mg) (P<0.01) (Figure 1I). These results suggest that the concentrations of the detected carotenoid pigments represent only a tiny fraction of total carotenoid content. Furthermore, the observed differences in carotenoids indicate that autotetraploidization may induce differences in carotenoid metabolism, which may be involved in the regulation of coloration and pigmentation.

Comparative analysis of differentially expressed genes

In this study, RCC and 4nRR represented the two extremes of coloration phenotypes. To investigate the molecular mechanisms affecting their coloration and pigmentation differences, skin transcriptome profiling was conducted on both groups (three RCC and three 4nRR) using RNA sequencing (RNA-Seq). This analysis yielded a total of 22 150 DEGs, including 20 681 up-regulated and 1 469 down-regulated DEGs (Supplementary Table S3 and Figure S1). To determine whether the pigmentation and coloration shifts in 4nRR were influenced by various biological pathways, enrichment and pathway analyses on these DEGs were conducted to pinpoint key genes involved in the signaling pathways responsible for pigmentation differences. Based on GO analysis, the DEGs between the RCC and 4nRR groups were enriched in 23 biological process terms, 17 cellular component terms, and 17 molecular function terms (Supplementary Table S4). The most significantly enriched terms were "Anatomical structure morphogenesis" and "Positive regulation of metabolic process" in the biological process category, "Macromolecular complex" and "Membrane-enclosed lumen" in the cellular component category, and "ATP binding" and "Enzyme binding" in the molecular function category (Supplementary Figures S2–S4), which were associated with metabolic, biological regulation and cellular

processes. Moreover, specific DEG sets were found to be enriched in carotenoid metabolism-related GO terms, including “Carotenoid dioxygenase activity”, “Scavenger receptor activity”, “Lipid metabolic process”, and “Integral component of membrane”. These findings suggest that the difference in carotenoid metabolism between RCC and 4nRR may contribute to the reduction in carotenoid content and variety in the skin of 4nRR, thereby regulating their distinct pigmentation and coloration profiles.

A total of 303 enriched pathways were identified through KEGG enrichment analysis (Supplementary Table S5), the top 20 of which are shown in Supplementary Figure S5. Of note, the DEGs were markedly enriched in endocytosis (ko04144), mTOR signaling pathway (ko04150), MAPK signaling pathway (ko04010), focal adhesion (ko04510), and phagosome (ko04145), which are related to lipid metabolism and signal transduction, consistent with the GO-enriched terms. The DEGs were also enriched in tyrosine metabolism (ko00350), melanogenesis (ko04916), and Wnt signaling pathway (ko04310), which significantly contribute to processes related to the formation and differentiation of pigment cells and melanin metabolism. These findings imply that melanin metabolism differs between RCC and 4nRR, potentially resulting in the existence of melanophores in the skin.

RT-qPCR verification of candidate carotenoid color genes

Based on analysis of differences in pigment cells, carotenoid pigments, and skin transcriptome enrichment between RCC and 4nRR, in conjunction with previously published research (Du et al., 2021; Yang et al., 2020), 28 essential DEGs implicated in red and yellow coloration were identified. A protein-protein interaction (PPI) network was constructed using the STRING tool to explore potential interactions among the proteins encoded by the DEGs. Cytoscape was then used to further identify candidate key genes. The interactome reconstructions indicated that among the 28 DEGs, 16 genes with interaction levels greater than 15 were identified as hub-genes (Figure 2A). To assess the reliability of the RNA-Seq results, gene expression profiling of the hub genes was conducted using RT-qPCR. Notably, 14 DEGs of the 16 qPCR-based tests yielded results consistent with the RNA-Seq findings, with four up-regulated and 10 down-regulated in the 4nRR group compared to the RCC group (Figure 2B),

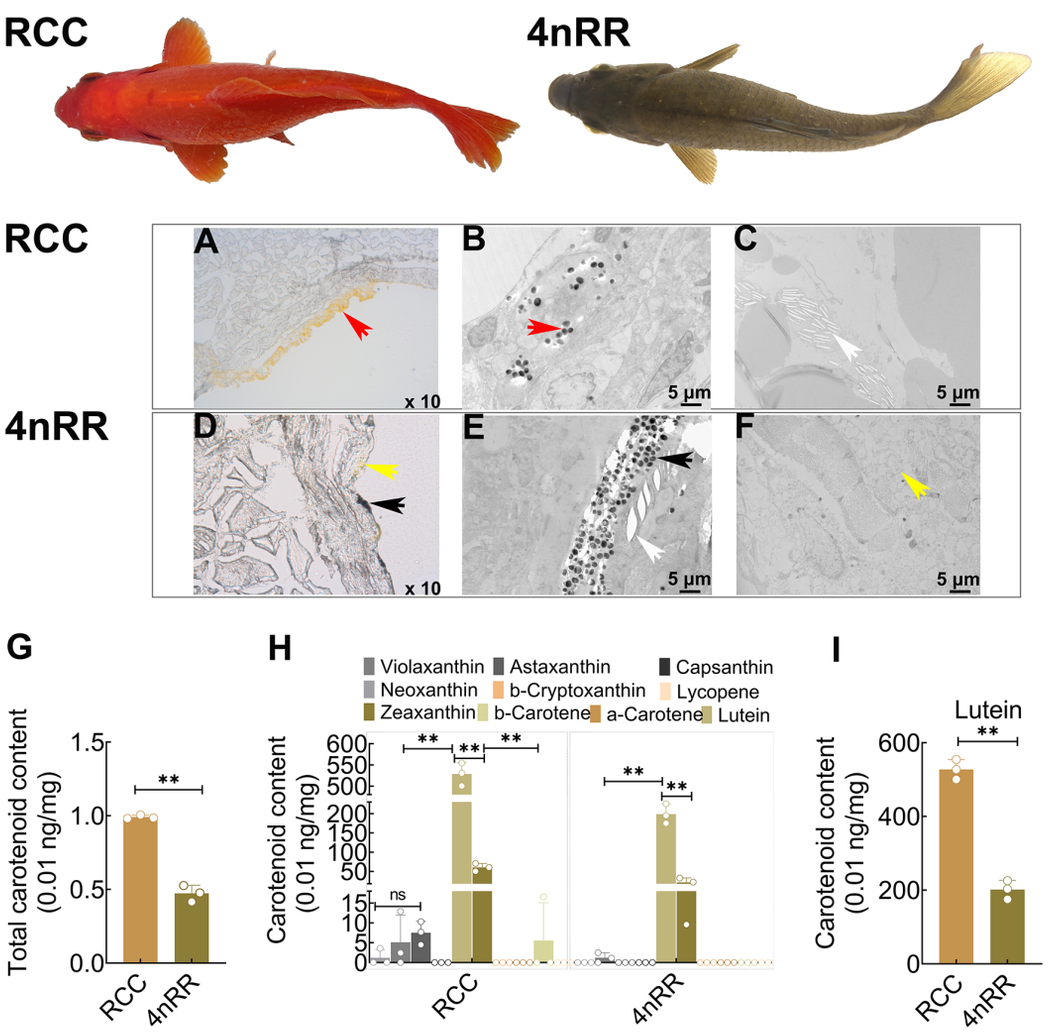

Figure 1 Determination of pigment cells and carotenoids in RCC and 4nRR skin

A, D: Cryosections of skin from RCC (A) and 4nRR (D). B, C, E, F: Ultrastructure of pigment cells. B, C: Erythrophores (B) and iridophores (C) in RCC. E, F: Melanophores with melanosomes, iridophores (E), and xanthophores (F) in 4nRR. Red, black, yellow, and white arrows sequentially point to erythrophores, melanophores, xanthophores, and iridophores. Bars are shown at bottom-right corner of images, black scale bar: 5 μm. G: Identification of total carotenoids between RCC and 4nRR. H: Detection of carotenoid pigments using UPLC in both RCC and 4nRR. I: Relative content of lutein in RCC and 4nRR. Asterisks indicate significant differences; ns: Not significant; *: $P<0.05$; **: $P<0.01$.

underscoring the reliability of the RNA-Seq results between the RCC and 4nRR groups. Moreover, transcript validation indicated a significant down-regulation in the expression of *scarb1* (P<0.01), an essential gene involved in carotenoid metabolism, in the 4nRR group compared with the RCC group, suggesting a vital role in coloration formation and pigmentation variation following autotetraploidization. Consequently, *scarb1* was designated as a candidate gene for subsequent study.

Identification and characterization of *scarb1* homeologs and alleles in 4nRR and RCC

Homology-based cloning yielded four *scarb1* transcripts from RCC and seven *scarb1* transcripts from 4nRR. These specific sequences were submitted to NCBI (OP466726 to OP466729 in RCC, OP466730 to OP466736 in 4nRR). Multiple nucleotide alignments and phylogenetic analysis clustered the four *scarb1* transcripts in RCC into two groups (two *scarb1a* and two *scarb1b*). The identities within the *scarb1a* and *scarb1b* groups were 99.13% and 99.34%, respectively, while the identities between *scarb1a* and *scarb1b* ranged from 82.96% to 86.82%. Post-autotetraploidization, 4nRR retained the CDS of *scarb1a* and *scarb1b*, as found in RCC, with another three transcripts annotated as duplicates. Consistently, the seven *scarb1* transcripts in 4nRR were grouped into four categories: two each for *scarb1a*, *scarb1b*, and *scarb1c*, and one for *scarb1d*. The two *scarb1c* transcripts only differed by a continuous 39 bp deletion on the 12th exon. The identities between *scarb1c* and *scarb1d* ranged from 91.42% to 93.93%. Except for *scarb1d* (*scarb1d-A*), two heterozygous alleles were identified for the other transcripts, annotated as *scarb1a-A*/*B*, *scarb1b-A*/*B*, and *scarb1c-A*/*B*. Amino acid sequence alignments revealed that *scarb1a-A*/*B* possessed the same amino acid, while *scarb1b-A*/*B* exhibited 98.81% identity (Figure 3A). These observations suggest that *scarb1a* and *scarb1b* may be a pair of homeologs derived

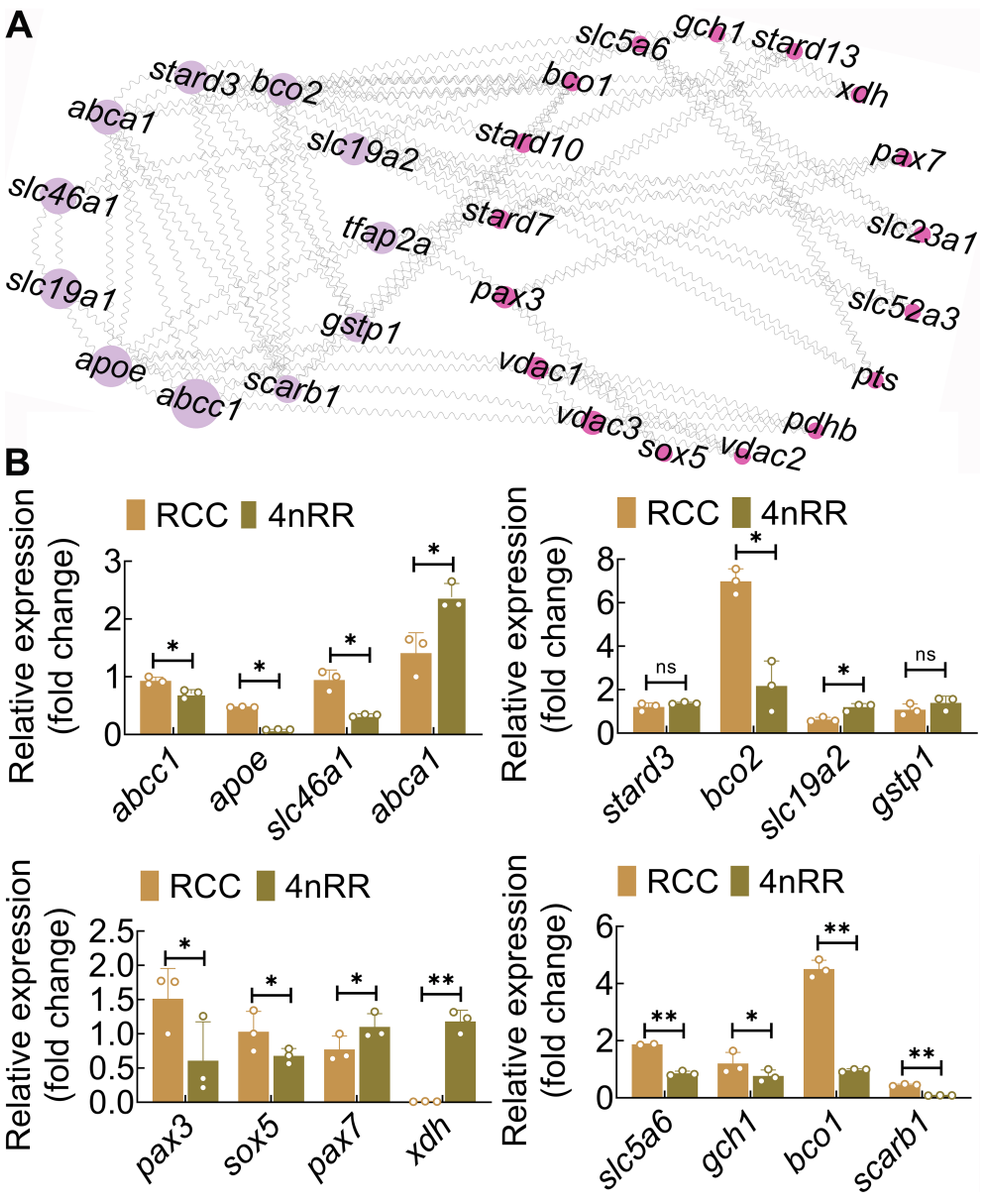

Figure 2 Identification of candidate hub genes related to red and yellow coloration

A: Protein-protein interaction network of red and yellow coloration-related genes in RCC and 4nRR groups. Genes with higher degree values are presented by a larger circle. B: RT-qPCR verification of hub genes. Data represent mean±standard deviation (SD), n=3 independent experiments. Significant differences are indicated by asterisks; ns: Not significant; *: P<0.05; **: P<0.01.

from early allotetraploidy (4R), whereas *scarb1c* and *scarb1d* emerged following autotetraploidization.

Interestingly, the identity between the duplicated *scarb1c* and *scarb1b* transcripts ranged from 91.42% to 93.93%, resulting in an amino acid identity of 92.46%. In contrast, the identity between the duplicated *scarb1d* and *scarb1a* transcripts ranged from 94.85% to 94.91%, with an amino acid identity of 93.36%. Additionally, the CDS and 3'-UTR lengths of *scarb1c-A* and *scarb1d-A* corresponded to those of *scarb1b* and *scarb1a*, respectively. Phylogenetic analysis indicated that the *scarb1* genes in fish clustered together, with the RCC and 4nRR *scarb1* genes sharing a higher degree of similarity with *Cyprinidae* than with other families. The *scarb1a* and *scarb1b* genes were grouped into two independent branches, suggesting ancestral duplication events in the RCC lineage (4R). Initially, *scarb1*c and *scarb1d* clustered with *scarb1-like* and *scarb1* of *Cyprinus carpio* var. *color*, respectively (*scarb1-like* shared 99.40% and 97.22% identities with *scarb1c-A* and *scarb1d-B*, respectively, while *scarb1* had 96.58% identity with *scarb1d-A*). Subsequently, they clustered with *scarb1b* and *scarb1a*, respectively, then clustered together after aggregating *Puntigrus tetrazona* with the branch where *scarb1c* was located (Figure 3B). These results suggest that, following autotetraploidization, *scarb1*c and *scarb1d* were duplicated from *scarb1b* and *scarb1a*, respectively, implying that the emergence of these duplicates may be functional.

To further determine the origin of amino acid variations in the duplicated *scarb1* genes of 4nRR, the sequences of *scarb1a* and *scarb1b* in RCC (RCC-*scarb1a* and RCC-*scarb1b*) and *scarb1* in *Megalobrama amblycephala* (BSB-*scarb1*) were used as controls. The statistical map of sites revealed distinct origins for the variant sites of *scarb1c* and *scarb1d*. Specifically, *scarb1c* was mainly derived from the fusion and recombination of *scarb1b* (35 sites), overlapping regions (22 sites) between *scarb1b* and BSB-*scarb1*, and its own mutations (15 sites). In contrast, *scarb1d* predominantly originated from *scarb1a* (34 sites), overlapping regions (10 sites) between *scarb1a* and BSB-*scarb1*, and its mutations (17 sites). Notably, a few variant sites in the duplicated *scarb1* homeologs originated solely from the fusion of BSB (four variant sites for *scarb1c* and three for *scarb1d*) (Figure 3A). The distribution of these variant sites revealed that after hybridization, the duplicated *scarb1* sequence was biased toward maintaining genetic stability.

Divergent expression patterns of *scarb1* homeologs and alleles

The expression characteristics of *scarb1* in the adult skin of RCC and 4nRR were analyzed using RT-qPCR. In the RCC skin, the transcript levels of *scarb1a* and *scarb1b* were high, with no significant differences between them (Figure 3C). In 4nRR, however, a distinct expression pattern was observed, with *scarb1a* showing 55.6 times higher expression than *scarb1b*, which exhibited extremely low expression (P<0.01) (Figure 3E). The transcript levels of all four *scarb1* homeologs were detected in 4nRR, with *scarb1a* showing the highest expression, followed by *scarb1d*, while *scarb1b* and *scarb1c* showed very low non-significant expression (Figure 3E).

To elucidate expression differences among the alleles of each *scarb1* homeolog (*scarb1a*, *scarb1b*, and *scarb1c*), cloning and sequencing were performed using specific SNPs for quantitative amplification. In RCC, an average of 85.7% of sequenced clones (30–36 clones for each individual, n=3) were attributed to *scarb1a-A*, while 14.3% corresponded to *scarb1a-B*. The expression of *scarb1b-B* was approximately 6.85-fold higher than that of *scarb1b-A*, constituting about six-sevenths of the total expression of *scarb1b-A/B* (Figure 3D). These findings suggest that *scarb1a* and *scarb1b* display a similar high expression level, with a marked bias in expression between their two alleles. Similarly, in 4nRR, the two alleles of *scarb1a*, *scarb1b*, and *scarb1c* also showed obvious biased expression, where *scarb1a-B* (76.9%), *scarb1b-B* (73.3%), and *scarb1c-B* (60%) showed dominant expression compared to their counterpart alleles, as evidenced by greater clone frequency and expression levels (Figure 3F). In contrast, *scarb1d* appeared to be homozygous or hemizygous, with no alleles detected. Thus, these results highlight the presence of differential allele expression.

Appearance of xanthophores and regional non-pigments in RCC under *scarb1* deficiency

Abundant *scarb1a* and *scarb1b* transcripts were amplified from RCC skin, indicating potential involvement in coloration regulation. To further clarify the regulation and interaction of the two *scarb1* homeologs in coloration and pigmentation, we generated individuals with singly and simultaneously disrupted *scarb1a* and *scarb1b* using CRISPR/Cas9. The *scarb1a* mutants (n=50), *scarb1b* mutants (n=50), and *scarb1a* and *scarb1b* double-mutants (n=50) were randomly sampled to identify genotypes and analyze pigmentation and histological skin characteristics. The sequencing results showed that the mutations of all F_0 individuals caused a reading frame shift. Interestingly, the F_0 individuals with either *scarb1a* (*scarb1a*$^{-2,\ \#2/-4}$+*scarb1b*$^{+/+}$) or *scarb1b* chimeric mutation (*scarb1a*$^{+/+}$+*scarb1b*$^{-7,\ -3/\#6,\ -10}$) exhibited almost identical phenotypic profiles, with red coloration turning to yellow (Figure 4). Moreover, cell biology analysis revealed the presence of xanthophores and iridophores in the skin of both chimeric mutants (Figure 4A–D). In the sequence analysis of disrupted *scarb1*, the two alleles of each gene exhibited in-frame mutations and deletions.

The *scarb1a* and *scarb1b* double mutants established by simultaneously disrupting two *scarb1* homeologs showed white or shallow-yellow streaks or patches embedded in the orange-yellow skin (Figure 5). Observations and imaging of skin sections showed xanthophores and erythrophores in the orange-yellow skin region (Figure 5E–G), xanthophores in the shallow-yellow skin region (Figure 5C, D), and only iridophores in the white region (Figure 5A, B). Moreover, since the area ratios of orange-yellow to lightly pigmented skin (white and shallow-yellow) among mutant individuals were distinguishing, ImageJ (Abràmoff et al., 2004) was used to calculate the area of lightly pigmented skin. Based on the reduction in the proportion of lightly pigmented skin area, these mutants were classified into two different phenotype groups (*scarb1a*$^{M24/M24}$+*scarb1b*$^{M24/M23}$ and *scarb1a*$^{M26/M26}$+*scarb1b*$^{M26/M28}$), with each group then sampled to detect the corresponding proportion of mutant sequences (out of 24–30 cloned sequences of each *scarb1*) (Supplementary Figure S6). Notably, 80% of *scarb1a*$^{M24/M24}$+*scarb1b*$^{M24/M23}$ individuals showed a higher proportion of lightly pigmented skin area, and contained only one WT sequence in *scarb1b-B*. Conversely, 20% of *scarb1a*$^{M26/M26}$+*scarb1b*$^{M26/M28}$ mutants showed a lower proportion of lightly pigmented skin area, and contained two WT sequences in *scarb1a-A*, *scarb1a-B*, and *scarb1b-A*, respectively. These results indicate that a higher quantity and

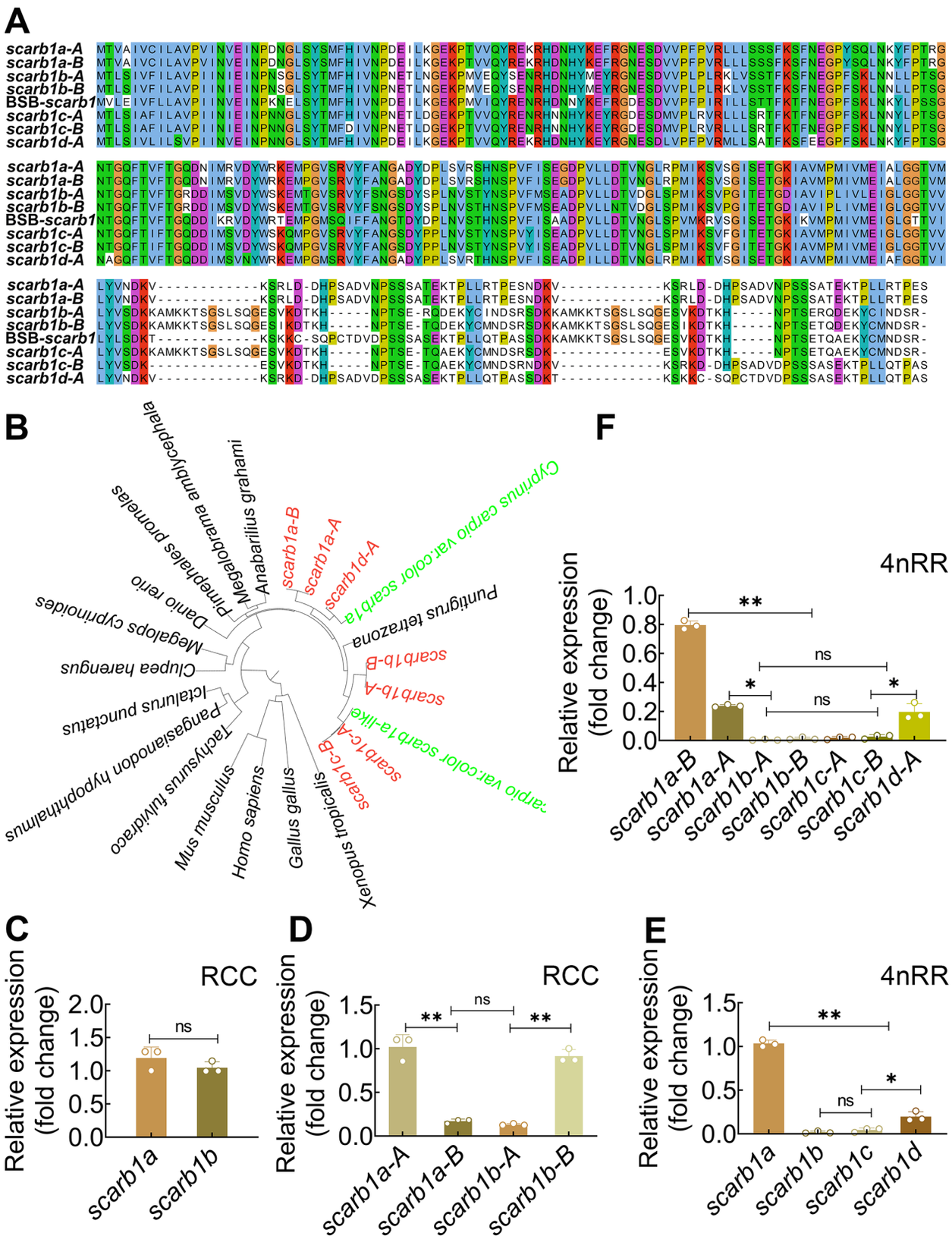

Figure 3 Identification and characterization of *scarb1* homeologs and alleles in RCC and 4nRR

A: Sites of amino acid variation alignments of duplicated *scarb1* homeologs, original *scarb1* homeologs, and BSB-*scarb1*. Consecutive dashes (-) represent position of amino acid deletions. B: Phylogenetic analysis of *scarb1* from RCC, 4nRR, and related species. Phylogenetic analysis was performed using the neighbor-joining method. C: Similar expression levels of two *scarb1* homeologs (*scarb1a* and *scarb1b*) in RCC. D: Expression differences between alleles of *scarb1* in RCC. E: Different expression patterns of four *scarb1* homeologs (*scarb1a*, *scarb1b*, *scarb1*c, and *scarb1d*) in 4nRR. F: Expression differences between alleles of *scarb1* in 4nRR. Asterisks indicate significant differences; ns: Not significant; *: $P<0.05$; **: $P<0.01$.

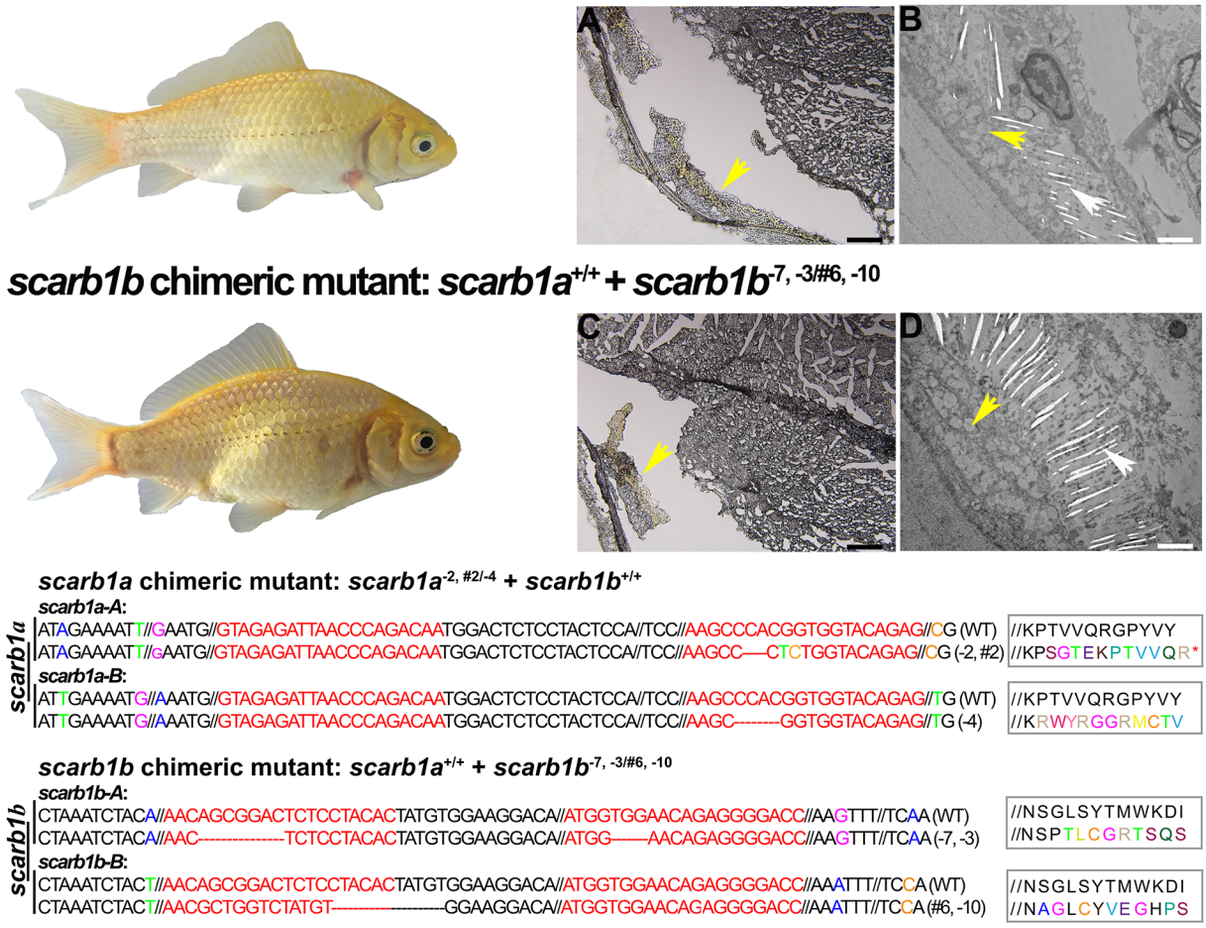

Figure 4 Phenotypes and genotypes of single *scarb1* homeolog knockout mutants in RCC

The *scarb1a* chimeric mutation (*scarb1a*$^{-2,\ \#2/-4}$+*scarb1b*$^{+/+}$) and *scarb1b* chimeric mutation (*scarb1a*$^{+/+}$+*scarb1b*$^{-7,\ -3/\#6,\ -10}$) exhibited almost identical phenotypic profiles. A–D: Yellow and white arrows point to xanthophores and iridophores, respectively. Bars are shown at bottom-right of images, black scale bar=10 μm, white scale bar=2 μm. Target sequence is marked in red; "-" and "#" represent deletion and substitution, respectively; "+/+" represents wild-type (WT) sequence; "//" represents the same nucleotide sequence among alleles.

proportion of WT sequences in *scarb1* may be involved in the formation and preservation of the yellow skin region.

The above findings suggest that disruption of either *scarb1a* or *scarb1b*, or both, may alter the composition of skin pigment cells, resulting in varied skin hue. Thus, *scarb1a* and *scarb1b* may be implicated in the formation of red coloration in RCC, acting in a gene dosage-dependent manner.

Generation of cyan-gray coloration phenotype in 4nRR via disruption of *scarb1* homeologs

In RCC, *scarb1a* and *scarb1b* exhibited higher expression levels and identical functions in coloration and pigmentation. In 4nRR, the divergent expression patterns observed between the original *scarb1* derived from RCC and the duplicated *scarb1* imply a potential divergence in their roles in regulating coloration and pigmentation. To explore the effect of both the original and duplicated *scarb1* genes on coloration in 4nRR, we generated individuals with singly and simultaneously disrupted *scarb1a*, *scarb1b*, *scarb1c*, and *scarb1d*. Interestingly, the single *scarb1*-mutated types displayed identical coloration features, with their body surface divided into brownish yellow and cyan-gray regions (Figure 6). The autotetraploid nature of 4nRR led to different complex mutations at the target sites within F_0 individuals. Based on specific SNPs in the two alleles of *scarb1a*, *scarb1b*, and *scarb1c*, the F_0 individuals were classified into specific mutated genotypes via sequence deletions and substitutions, including *scarb1a* chimeric mutants (*scarb1a*$^{-1,\ \#2/-5}$+*scarb1b*$^{+/+}$+*scarb1c*$^{+/+}$+*scarb1d*$^{+}$) (*n*=30), *scarb1b* chimeric mutants (*scarb1a*$^{+/+}$+*scarb1b*$^{-5,\ -3,\ -3/+3,\ \#2,\ -5}$+*scarb1c*$^{+/+}$+*scarb1d*$^{+}$) (*n*=30), *scarb1c* chimeric mutants (*scarb1a*$^{+/+}$+*scarb1b*$^{+/+}$+*scarb1c*$^{\#10/-8}$+*scarb1d*$^{+}$) (*n*=30), and *scarb1d* chimeric mutants (*scarb1a*$^{+/+}$+*scarb1b*$^{+/+}$+*scarb1c*$^{+/+}$+*scarb1d*$^{-10,\ \#3}$) (*n*=30) (Supplementary Figure S7). Histological observations of skin pigment cells revealed that melanophores, iridophores, and xanthophores still coexisted in the brownish-yellow skin (Figure 6D–F), while only melanophores and iridophores were present in the cyan-gray skin (Figure 6A–C).

The F_0 individuals with simultaneous *scarb1a*, *scarb1b*, *scarb1c*, and *scarb1d* mutations were also obtained by co-injection of their specific sgRNAs with the Cas9 protein. Among the quadruple-mutants, two types of mutants (*scarb1a*$^{M25/M25}$+*scarb1b*$^{M25/M25}$+*scarb1c*$^{M25/M25}$+*scarb1d*^{M25}, Type I, and *scarb1a*$^{M25/M25}$+*scarb1b*$^{M25/M23}$+*scarb1c*$^{M24/M24}$+*scarb1d*^{M24}, Type II) were observed with apparent differences in coloration. One variant, representing approximately 1% (*n*=2), displayed extensive cyan-gray coloration, while the

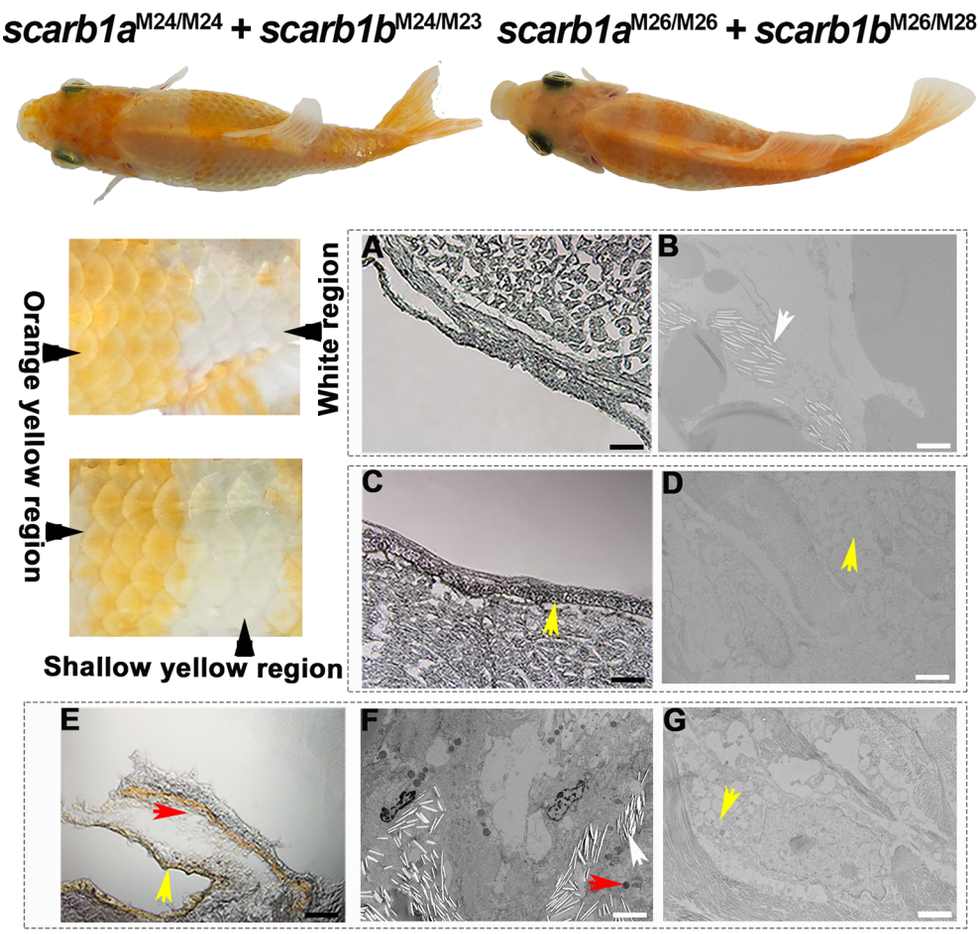

Figure 5 Different phenotype groups of *scarb1* double-mutated individuals in RCC

Mutant (*scarb1a*$^{M24/M24}$+*scarb1b*$^{M24/M23}$) contained a higher proportion of lightly pigmented skin. Mutant (*scarb1a*$^{M26/M26}$+*scarb1b*$^{M26/M28}$) contained a lower proportion of lightly pigmented skin. A, B: Iridophores in white region. C, D: Xanthophores in shallow-yellow skin region. E–G: Xanthophores, erythrophores, and iridophores in orange-yellow skin region. Red, yellow, and white arrows point to erythrophores, xanthophores, and iridophores, respectively. Bars are shown at bottom-right of images, black scale bar=10 μm, white scale bar=2 μm.

other variant, constituting around 99% (*n*=200), showed a similar coloration pattern to the single chimeric mutants, although the proportion of cyan-gray to brownish-yellow skin was higher than in any single-mutated individual (Figure 7). Melanocytes and iridophores were only observed in the skin of the former (Figure 7A, B), and analysis of DNA clones revealed the absence of any WT *scarb1* sequences in these mutants (25 clones) (Supplementary Figure S8). Conversely, the skin of the more common variant featured pigment cell types identical to those found in the chimeric mutants (Figure 7C–E), and analysis showed the presence of more WT *scarb1* sequences compared to the first variant, alongside non-WT sequences (Supplementary Figure S8).

In conclusion, in 4nRR, disruption of any one of the four *scarb1* homeologs resulted in the local alteration of skin pigmentation. In contrast, simultaneous knockout of all *scarb1* genes led to the development of a cyan-gray mutant and a like-chimeric mutant. These findings demonstrate that, in autotetraploid *Carassius auratus*, both the original *scarb1* derived from *Carassius auratus* red var. and the *scarb1* genes duplicated by autotetraploidization are deeply involved in coloration formation, with the four homologous *scarb1* genes also exhibiting a gene-dosage effect.

Compensation of body color-related genes in localized coloration of F_0 mutated individuals

In both *scarb1* single-mutated and multiple-mutated individuals, partial skin regions exhibited yellow or orange-yellow coloration in RCC and brownish-yellow coloration in 4nRR. Given the observed variations in coloration and pigmentation, which are intricately tied to a complex molecular regulatory network, we hypothesized that specific skin colorations may result from the synergistic activity of pigment-related genes. We first examined the expression of remaining intact *scarb1* in *scarb1* single-mutated individuals, then focused on the expression patterns of genes associated with red or yellow coloration in *scarb1* multiple-mutated individuals. In RCC skin, expression analysis revealed significant up-regulation of *scarb1b* in *scarb1a* chimeric mutants (3.3–25.3-fold higher compared to WT skin) (Figure 8A) and of *scarb1a* in *scarb1b* chimeric mutants (3.3–25.3-fold higher compared to WT skin) (Figure 8D). Similarly, in 4nRR, the three intact *scarb1* homeologs were also detected in the *scarb1* single-mutated individuals, showing a marked up-regulation in expression compared to WT 4nRR (Figure 8B, C, E, F). These results suggest a compensatory up-regulation of *scarb1* in affected skin regions of F_0 mutants, likely contributing to the preservation of yellow and brownish-yellow coloration.

In addition, compared with the orange-yellow skin in RCC, 10 red or yellow coloration-related genes (*abcc1*, *apoe*, *slc46a1*, *abca1*, *gstp1*, *pax3*, *sox5*, *pax7*, *gch1*, and *bco1*) exhibited substantially lower expression in lightly pigmented

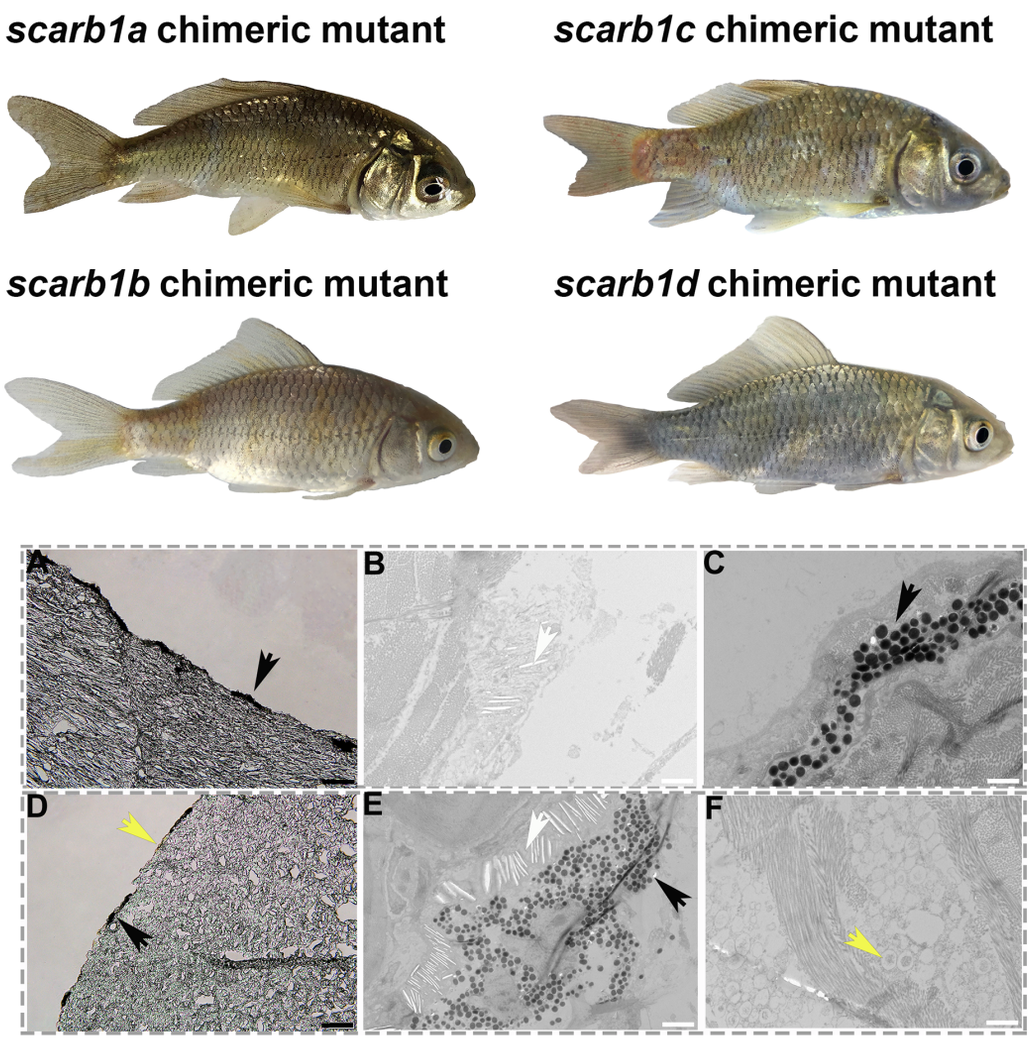

Figure 6 Phenotype of single *scarb1* homeolog knockout 4nRR individuals

The *scarb1a* chimeric mutant (*scarb1a*$^{-1,\ \#2/-5}$+*scarb1b*$^{+/+}$+*scarb1c*$^{+/+}$+*scarb1d*$^{+}$), *scarb1b* chimeric mutant (*scarb1a*$^{+/+}$+*scarb1b*$^{-5,\ -3,\ -3/+3,\ \#2,\ -5}$+*scarb1c*$^{+/+}$+*scarb1d*$^{+}$), *scarb1c* chimeric mutant (*scarb1a*$^{+/+}$+*scarb1b*$^{+/+}$+*scarb1c*$^{\#10/-8}$+*scarb1d*$^{+}$), and *scarb1d* chimeric mutant (*scarb1a*$^{+/+}$+*scarb1b*$^{+/+}$+*scarb1c*$^{+/+}$+*scarb1d*$^{-10,\ \#3}$) showed identical coloration features. A–C: Melanophores and iridophores in cyan-gray region. D–F: Melanophores, xanthophores, and iridophores in brownish-yellow region. Black, yellow, and white arrows point to melanophores, xanthophores, and iridophores, respectively. Bars are shown at bottom-right of images, black scale bar=10 μm, white scale bar=2 μm.

skin, while three genes (*bco2*, *vdad3*, and *xdh*) were remarkably up-regulated (Figure 8G, H). Similarly, for the 4nRR mutants, relative to the brownish-yellow skin, nine genes associated with red or yellow coloration (*abcc1*, *apoe*, *slc46a1*, *abca1*, *stard3*, *gch1*, *gstp1*, *bco1*, and *xdh*) demonstrated notable reductions in expression within the cyan-gray coloration regions, while three genes (*bco2*, *vdad3*, and *sox5*) displayed marked increases (Figure 8I, J). These results imply the occurrence of similar gene expression patterns in RCC and 4nRR, indicating that appropriate shifts in the expression of these pigment-related genes may play a role in maintaining yellow coloration in both fish.

DISCUSSION

Animal coloration and pigment patterns are shaped by the synthesis of different pigments and the unique distribution of diverse chromatophores. Chromatophores, cells containing pigment and reflecting light, are responsible for synthesizing and storing pigments, such as melanin, pteridines, and carotenoids (Cuthill et al., 2017; Fujii, 2000; Rashidian et al., 2021). In this study, chromatophores were found to be distributed differently between the two fish types, with erythrophores and iridophores present in RCC skin, but melanophores, xanthophores, and iridophores present in 4nRR skin. These findings suggest that the composition and distribution of chromatophores are key factors in the observed changes in pigmentation and coloration in 4nRR. In fish, the regulation, transportation, and deposition of different pigments in chromatophores play critical roles in the diversity and complexity of coloration and pigment patterns (Čupić et al., 2023; Johnson & Fuller, 2015). Colors that range from yellow to red predominantly arise from carotenoids and pteridines stored in xanthophores/erythrophores. Carotenoids generally encompass a mix of different compounds deposited in specific pigment cells either directly through the diet or through endogenous metabolic conversions, with red-colored organisms typically exhibiting a higher carotenoid content compared to those with a reddish or yellowish hue (Elmadfa & Majchrzak, 1998; Lin et al., 2010; Liu et al., 2012; Ng'oma et al., 2014; Ohkubo et al., 1999). Our study revealed distinct differences in the composition and concentration of carotenoids between RCC and 4nRR, primarily showing

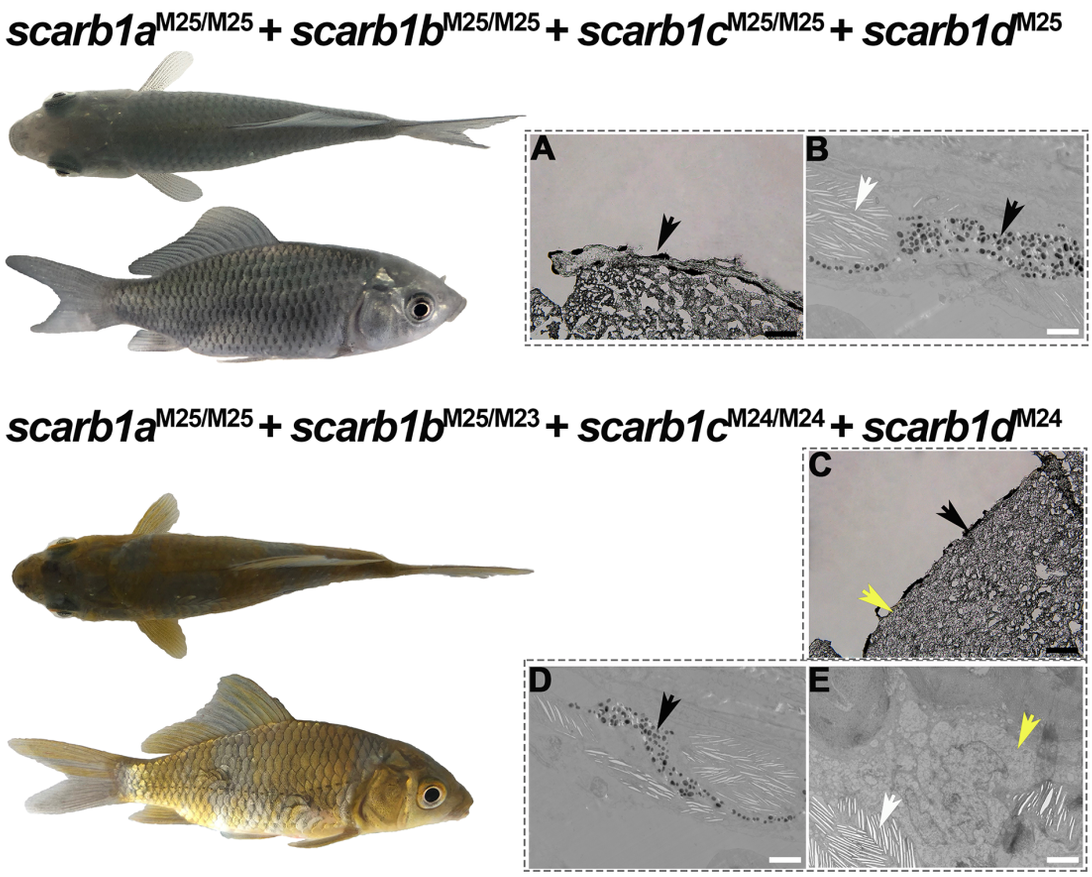

Figure 7 Phenotype of individuals subjected to simultaneous *scarb1a*, *scarb1b*, *scarb1c*, and *scarb1d* mutation

Two mutants include *scarb1a*$^{M25/M25}$+*scarb1b*$^{M25/M25}$+*scarb1c*$^{M25/M25}$+*scarb1d*^{M25} and *scarb1a*$^{M25/M25}$+*scarb1b*$^{M25/M23}$+*scarb1c*$^{M24/M24}$+*scarb1d*^{M24}. A, B: Pigment cells of mutant (*scarb1a*$^{M25/M25}$+*scarb1b*$^{M25/M25}$+*scarb1c*$^{M25/M25}$+*scarb1d*^{M25}). C–E: Pigment cells of mutant (*scarb1a*$^{M25/M25}$+*scarb1b*$^{M25/M23}$+*scarb1c*$^{M24/M24}$+*scarb1d*^{M24}). "M" indicates "mutant sequences" (n=25). Black, yellow, and white arrows point to melanophores, xanthophores, and iridophores, respectively. Bars are shown at bottom-right of images, black scale bar=10 μm, white scale bar=2 μm.

significantly higher total carotenoid content and composition in RCC than in 4nRR, pointing to pronounced differences in carotenoid metabolism. Given the lipid solubility and high hydrophobicity of carotenoids (Granneman et al., 2017; Von Lintig et al., 2020), we postulate that autotetraploidization may have led to differences in carotenoid metabolism, resulting in changes in erythrophores and xanthophores.

Carotenoid-based coloration exhibits significant potential for plasticity. However, recent advancements in transcriptomics, whole-genome sequencing, and the identification of genes involved in carotenoid ornamentation suggest that genetic factors play a crucial role in carotenoid-based coloration and patterns (Toews et al., 2017; Yang et al., 2020). Here, based on comparative transcriptomic analysis of the red skin regions in RCC and brownish-yellow skin regions in 4nRR, we identified 22 150 DEGs and several critical pathways associated with lipid homeostasis, pigmentation, retinol metabolism, pigment cell formation and differentiation, and melanin metabolism, offering insights into the potential molecular mechanisms underlying coloration changes. Analysis of the 16 hub genes involved in pteridine and carotenoid metabolism revealed higher expression of *abca1* and significantly lower expression of *scarb1* in 4nRR compared to RCC, indicating they were differentially expressed in carotenoid transport between the two fish species (Figure 2B). Furthermore, compared to RCC, *gstp1* and *stard3*, associated with carotenoid binding and deposition, showed increased expression in 4nRR, while *bco1* and *bco2*, responsible for carotenoid breakdown, showed decreased expression. Previous studies have shown that *abca1* is associated with lipid efflux, cholesterol transport, and high-density lipoprotein (HDL) secretion, and its mutation can result in the deficiency of lutein and zeaxanthin in the blood and peripheral tissue of chickens (Connor et al., 2007). Our results showed that both fish contained lutein and zeaxanthin, but the level of lutein, the most abundant carotenoid pigment detected, was significantly reduced in 4nRR. Additionally, *abca1* was up-regulated in the brownish-yellow skin of 4nRR, suggesting it may not be responsible for carotenoid metabolism in 4nRR. As a member of class B scavenger receptors, *scarb1* is concerned with the uptake and transport of carotenoids by binding to chemically modified lipoproteins or other anion ligands (Plüddemann et al., 2007). Previous studies have shown that *scarb1* is essential in carotenoid metabolism in *Drosophila* eyes, for the yellow feathers in birds, for the red skin in Oujiang color common carp (*Cyprinus carpio* var. *color*), and for the pink and red muscles in salmon (Du et al., 2021; Kiefer et al., 2002; Sundvold et al., 2011; Toomey et al., 2017). Furthermore, *scarb1* is reported to selectively absorb *β*-carotene in the duodenum of mice (Van Bennekum et al., 2005). Interestingly, *β*-carotene was detected in the red skin of RCC but was absent in the brownish-yellow skin of 4nRR. Correspondingly, *scarb1* showed significantly lower expression in 4nRR than in RCC, suggesting that the regulation of *scarb1* may have changed after autotetraploidization. StAR-related lipid transfer domain

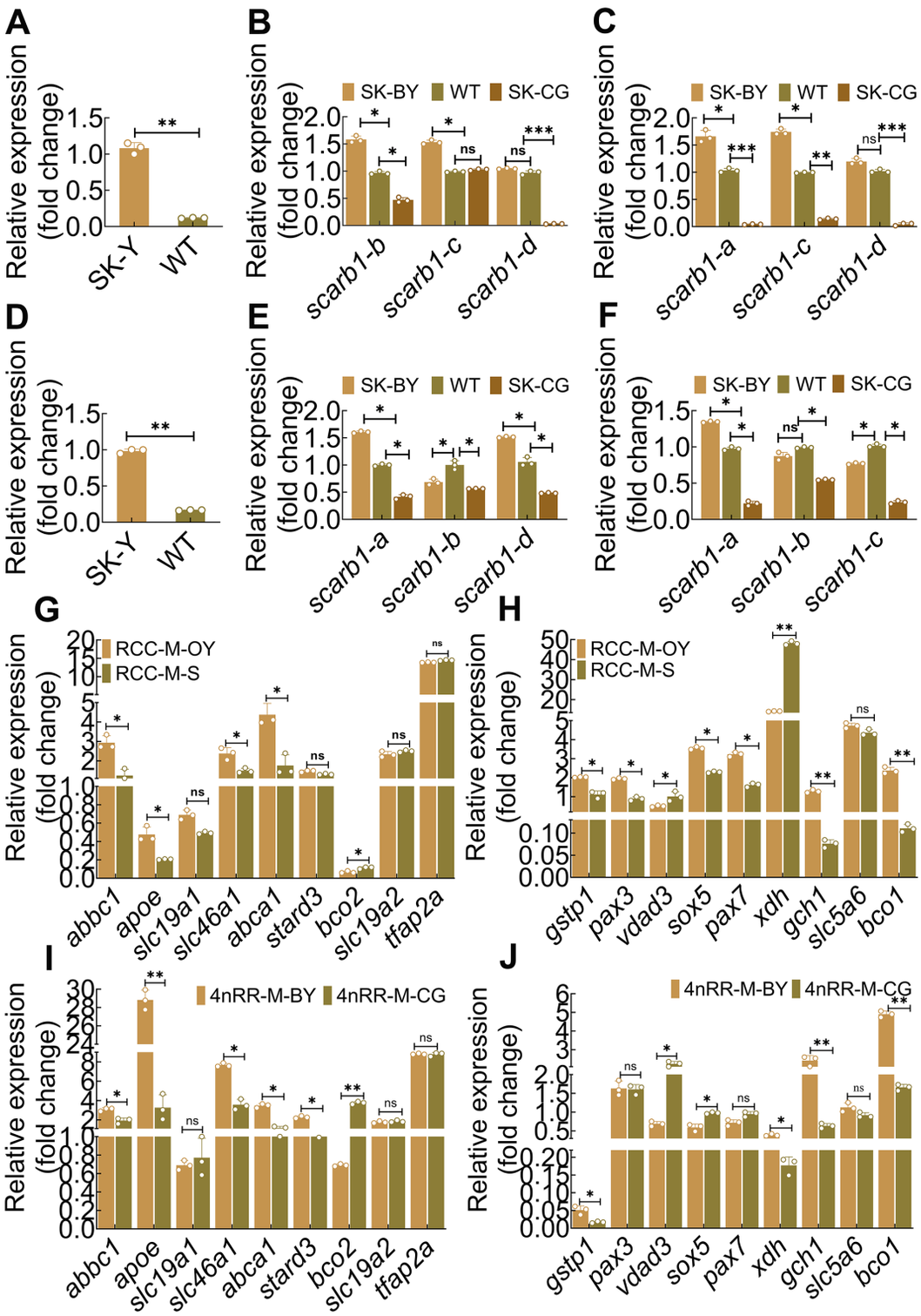

Figure 8 Relative expression levels of intact *scarb1* or red or yellow coloration-related genes in mutant individuals

A, B: Expression levels of *scarb1b* (A) and *scarb1a* (D) in *scarb1a* and *scarb1b* chimeric RCC mutants, respectively. B, C, E, F: Expression levels of other three intact *scarb1* homeologs in *scarb1a* (B), *scarb1b* (C), *scarb1c* (E), and *scarb1d* (F) chimeric 4nRR mutants. G, H: Relative expression of red or yellow coloration-related genes in lightly pigmented skin and orange-yellow skin of RCC. I, J: Relative expression of genes associated with red or yellow coloration in cyan-gray and brownish-yellow skin of 4nRR. Asterisks indicate significant differences; ns: Not significant; *: P<0.05; **: P<0.01.

containing 3 (*stard3*) is a membrane-associated protein responsible for regulating intracellular lipid metabolism and specifically binding luteinizing hormone in the human retina (Li et al., 2011). Acting as a zeaxanthin binding protein, *gstp1* is associated with the absorption of lutein and zeaxanthin in the human retina (Bhosale et al., 2004). In our study, both *stard3* and *gstp1* were up-regulated in 4nRR skin. Reduced expression of *bco2* leads to the accumulation of carotenoids in birds, whereas an increase in *bco2a* expression has been noted in the white skin compared to the yellow skin of East

African cichlid fish. (Ahi et al., 2020; Gazda et al., 2020). Our results showed that *bco1* and *bco2* were both down-regulated in 4nRR, consistent with previous studies in salmon (Ahi et al., 2020; Lehnert et al., 2019) and domestic chickens (Eriksson et al., 2008). In the pteridine synthesis pathway, substrate guanosine triphosphate (GTP) is converted by *gch1*, followed by 6-pyruvoyl tetrahydropterin synthase (PTPS) into 6-pyruvoyl-H4-pterin, with drosopterin, sepiapterin, and H4-biopterin (BH4) then synthesized specifically. BH4 is also involved in pteridine and melanin synthesis, acting as a co-factor to inhibit GCHFR activity and promote L-DOPA synthesis (Braasch et al., 2007). Here, however, *gch1* was expressed at lower levels in the brownish-yellow containing melanophores and xanthophores, suggesting that this gene may not have a significant effect on 4nRR. Additionally, *xdh*, essential in the synthesis of 7-oxobiopterin, isoxanthopterin, and 2,4,7-trioxopteridine (Leclercq et al., 2010) and found to be up-regulated in the xanthophores of zebrafish (Le et al., 2005), was also up-regulated in 4nRR, suggesting it may have a positive effect on pteridine in 4nRR. However, whether pteridine exists in 4nRR needs to be confirmed in further experiments. Collectively, these findings suggest that the coloration variation observed between RCC and 4nRR is closely related to carotenoid metabolism. Given the known functions of these genes and the expression differences between RCC and 4nRR, *scarb1* (P<0.01) was selected as the target gene for subsequent experiments.

Fish exhibit a remarkable diversity in colors and pigment patterns, largely attributed to FSGD. Studies have shown that pigmentation-related genes were preferentially preserved following FSGD, resulting in teleost fish having about 30% more pigmentation-related genes than tetrapods (Braasch et al., 2009). In addition to FSGD, polyploidy events have also occurred repeatedly in certain taxonomic fish orders (Gui & Zhou, 2010; Leggatt & Iwama, 2003). The amphidiploid *Carassius auratus* red var. is thought to have originated from an allotetraploidy event. Previous studies have reported that subgenomic evolution in *Carassius auratus* red var. shifted from asymmetrical to balanced genomic diversification during rediploidization (Luo et al., 2020). Our analysis uncovered two highly similar *scarb1* homeologs in RCC, which were organized into distinct branches in the phylogenetic tree, suggesting ancestral gene duplication in RCC (4R). The 4nRR genome was derived from a WGD event in RCC. Previous studies have shown that the genome of synthesized autotetraploid *Carassius auratus* undergoes rapid genetic and epigenetic modifications (Wang et al., 2020a). Furthermore, analyses have revealed variations in genetic composition, particularly in duplicated genes post-autotetraploidization, while also retaining original genes from RCC (Huang et al., 2020; Qin et al., 2019b). Similarly, our study identified differences in genetic composition between the two original *scarb1* homeologs and two duplicated homeologs in 4nRR, consistent with previous analysis. Interestingly, amino acid variations were noted in duplicated *scarb1c* and *scarb1d*, which were respectively derived from the fusion and recombination of *scarb1b* and BSB-*scarb1* and of *scarb1a* and BSB-*scarb1*, hinting at a hybrid origin of the *scarb1* paralogs in 4nRR. Such parental-derived sequence variations and homoeologous recombinations have been reported in newly formed allopolyploid fish and other newly synthesized polyploid plants during polyploidy formation (Martelotto et al., 2007; Mecchia et al., 2007; Qin et al., 2019a; Ren et al., 2022; Song et al., 1995), leading to divergence between homologous genes and increased heterozygosity, potentially enhancing genetic balance and stability across subgenomes.

Hybridization and polyploidization can link cis-acting elements from different promoter and enhancer sources, thereby regulating gene expression in polyploid genomes. This mechanism is beneficial for the formation of polyploids, particularly for genome stability and rapid environmental adaptation. In allopolyploids, syntenic gene pairs often display homoeologous expression bias. For example, pairwise comparisons between syntenic gene pairs in *Eragrostis tef* show a slight bias in transcript expression toward the B subgenome, with the most significant bias occurring in severely drought-stressed leaves, suggesting an adaptation to adverse environments (VanBuren et al., 2020). Similar patterns of homeolog expression bias have also been reported in allotetraploid *Brassica juncea*, *Gossypium hirsutum* L. acc. TM-1, triploid maize, and nascent allotetraploid fish lineages (Ren et al., 2022; Yang et al., 2016; Yao et al., 2013; Zhang et al., 2015). In 4nRR, a distinct expression imbalance was observed in homologous genes between the A and A' homologous genomes, with a notable switch in dominant gene expression during embryonic development (unpublished). Further analysis of *scarb1* homologous gene expression in 4nRR showed clear bias (*scarb1a*>*scarb1d*>*scarb1b*=*scarb1c*), with original *scarb1a* displaying dominant expression, underscoring its crucial role in pigmentation. Interestingly, analysis of allele-specific expression (ASE) revealed that *scarb1* was detected in both RCC (85.7% for *scarb1a-A* and 14.3% for *scarb1a-B*; 12.5% for *scarb1b-A* and 87.5% for *scarb1b-B*) and 4nRR (76.9% for *scarb1a-A*, 73.3% for *scarb1b-A*, and 60% for *scarb1c-A*). ASE, often driven by cis-regulatory elements, is a common event in various animal species, including humans, mice, chickens, Amazon mollies, California tiger salamanders, and hybrid tilapias (Cooper & Shaffer, 2021; Lagarrigue et al., 2013; Lo et al., 2003; Song et al., 2012b; Zhou et al., 2019; Zhu et al., 2017; Zhuo et al., 2017). These occurrences have been linked to disease risk and phenotypic severity of disease-causing CDS variants. Research has also shown that 18% of genes in triploid *Oryzias latipes* exhibit a wide range of ASE levels (Garcia et al., 2014). Overall, our study provides novel insights into ASE in 4nRR, which may help explain the implications of genetic variation on ASE after autotetraploidization.

The impact of WGDs on the emergence of new traits, ecological adaptations, speciation, and increased biodiversity is well-recognized, highlighting its crucial role as a driving force in eukaryotic evolution (Soltis & Soltis, 2016; Van De Peer et al., 2017; Zhou & Gui, 2017). WGDs serve as a crucial source of genetic diversity, offering a basis for generating novel gene functions that enhance an organism's evolutionary adaptation and complexity. The primary outcomes of WGDs on duplicated gene function include pseudogenization, resulting in gene function loss, neofunctionalization, resulting in novel gene function gain, and subfunctionalization, resulting in the retention of partial ancestral gene function (Cheng et al., 2018). Amphidiploid *Carassius auratus* red var. and autotetraploid *Carassius auratus*, which originated from a WGD event in *Carassius auratus* red var., are ideal models for studying the function and differentiation of duplicated genes. Herein, we achieved single-homeolog and multi-homeolog knockout in both RCC and 4nRR using CRISPR/Cas9. Results showed that disruption of any single homologous

gene in either RCC or 4nRR led to an alteration in coloration. This confirmed that duplicated *scarb1* genes, like the original *scarb1* genes, are indeed the causal genes associated with brownish-yellow phenotypes, having undergone subfunctionalization to synergistically and equally govern pigmentation. This represents a novel finding of functional differentiation of duplicated genes in autotetraploid fish. Importantly, in both RCC and 4nRR, *scarb1* multiple-mutated individuals showed a significantly higher deficiency in pigment cells and a greater area of color variation than single-mutated individuals. Notably, multiple-mutated individuals harboring more non-WT sequences exhibited higher ratios of coloration variation. Additionally, the three intact *scarb1* homeologs in the single-mutated chimeric individuals showed markedly higher expression than in the WT fish. These results suggest that *scarb1* homeologs act synergistically through a gene dosage-compensation effect to influence coloration and pigmentation. Gene dosage, a central aspect of WGD events, is believed to be a coordinated response to duplications, with complex gene dosage compensation reported in vertebrates to ensure the appropriate regulation of gene products and enhance adaptive evolution (Song et al., 2020; Veitia & Birchler, 2022). Studies have shown that retained gene groups exhibit better dosage response coordination in autotetraploid and allotetraploid *Arabidopsis thaliana* (Mattingly & Hovick, 2023). Additionally, significant gene dosage selection has been documented in four salmonid species (Gillard et al., 2021), and dosage compensation has been identified in triploid hybrid fish (Li et al., 2018; Ren et al., 2017). In our study, the *scarb1* homeologs exhibited functional additivity in both fish species, implying that other intact *scarb1* homeologs may play a compensatory role in maintaining yellow skin in RCC and brown-yellow skin in 4nRR. Additionally, we analyzed the expression levels of carotenoid and pteridine-related genes in response to observations that some skin regions of *scarb1* multiple-mutated individuals retained the WT coloring. Our results showed that both RCC and 4nRR exhibited similar gene expression patterns, with appropriate and explainable up- and down-regulation. Based on our findings, we propose that in addition to the mosaic nature of the mutants, the expression of these pigment-related genes may also contribute to the retention of WT coloration in both fish. However, further studies, including complementarity assays, are necessary to determine whether the retention of WT coloration in mutants is due to their mosaic nature or some compensatory genetic mechanism.

DATA AVAILABILITY

The obtained *scarb1* gene sequences are available from the NCBI (*scarb1a-A* GenBank: OP466726, *scarb1a-B* GenBank: OP466727, *scarb1b-A* GenBank: OP466728, and *scarb1b-B* GenBank: OP466729) and 4nRR (*scarb1a-A* GenBank: OP466730, *scarb1a-B* GenBank: OP466731, *scarb1b-A* GenBank: OP466732, *scarb1b-B* GenBank: OP466733, *scarb1c-A* GenBank: OP466734, *scarb1c-B* GenBank: OP466735, and *scarb1d-A* GenBank: OP466736), GSA database (https://ngdc.cncb.ac.cn/gsa/, CRA014084), and Science Data Bank database (https://www.scidb.cn/c/zoores, CSTR: 31253.11.sciencedb.j00139.00097).

SUPPLEMENTARY DATA

Supplementary data to this article can be found online.

COMPETING INTERESTS

The authors declare that they have no competing interests.

AUTHORS' CONTRIBUTIONS

Q.B.Q. designed the study and S.J.L. provided expert comments. X.D.X. provided the preliminary data that supported this study. Y.Z., X.H., L.W.H., X.Y.Z., X.Z.F., and M.M. performed the daily animal care. C.Q.W., K.Z., and X.W.X. analyzed the data. X.D.X. wrote the manuscript. All authors read and approved the final version of the manuscript.

REFERENCES

Abràmoff MD, Magalhães P, Ram SJ. 2004. Image processing with ImageJ. *Biophotonics International*, **11**(7): 36−42.

Ahi EP, Lecaudey LA, Ziegelbecker A, et al. 2020. Comparative transcriptomics reveals candidate carotenoid color genes in an East African cichlid fish. *BMC Genomics*, **21**(1): 54.

Awan MJA, Rasheed A, Saeed NA, et al. 2022. *Aegilops tauschii* presents a genetic roadmap for hexaploid wheat improvement. *Trends in Genetics*, **38**(4): 307−309.

Bagnara JT, Matsumoto J. 2006. Comparative anatomy and physiology of pigment cells in nonmammalian tissues. *In*: Nordlund JJ, Boissy RE, Hearing VJ, et al. The Pigmentary System: Physiology and Pathophysiology. Hoboken: Blackwell, 11–59.

Bhosale P, Larson AJ, Frederick JM, et al. 2004. Identification and characterization of a pi isoform of glutathione *S*-transferase (GSTP1) as a zeaxanthin-binding protein in the macula of the human eye. *Journal of Biological Chemistry*, **279**(47): 49447−49454.

Braasch I, Brunet F, Volff JN, et al. 2009. Pigmentation pathway evolution after whole-genome duplication in fish. *Genome Biology and Evolution*, **1**: 479−493.

Braasch I, Schartl M, Volff JN. 2007. Evolution of pigment synthesis pathways by gene and genome duplication in fish. *BMC Evolutionary Biology*, **7**(1): 74.

Chen ZJ, Sreedasyam A, Ando A, et al. 2020. Genomic diversifications of five *Gossypium* allopolyploid species and their impact on cotton improvement. *Nature Genetics*, **52**(5): 525−533.

Chen ZL, Omori Y, Koren S, et al. 2019. De novo assembly of the goldfish (*Carassius auratus*) genome and the evolution of genes after whole-genome duplication. *Science Advances*, **5**(6): eaav0547.

Cheng F, Wu J, Cai X, et al. 2018. Gene retention, fractionation and subgenome differences in polyploid plants. *Nature Plants*, **4**(5): 258−268.

Clotfelter ED, Ardia DR, Mcgraw KJ. 2007. Red fish, blue fish: trade-offs between pigmentation and immunity in *Betta splendens*. *Behavioral Ecology*, **18**(6): 1139–1145.

Connor WE, Duell PB, Kean R, et al. 2007. The prime role of HDL to transport lutein into the retina: evidence from HDL-deficient WHAM chicks having a mutant ABCA1 transporter. *Investigative Ophthalmology & Visual Science*, **48**(9): 4226−4231.

Cooper RD, Shaffer HB. 2021. Allele-specific expression and gene regulation help explain transgressive thermal tolerance in non-native hybrids of the endangered California tiger salamander (*Ambystoma californiense*). *Molecular Ecology*, **30**(4): 987−1004.

Corneillie S, De Storme N, Van Acker R, et al. 2019. Polyploidy affects plant growth and alters cell wall composition. *Plant Physiology*, **179**(1): 74−87.

Čupić M, Marčić Z, Lukić M, et al. 2023. The first cavefish in the Dinaric Karst? Cave colonization made possible by phenotypic plasticity in *Telestes karsticus*. *Zoological Research*, **44**(4): 821–833.

Cuthill IC, Allen WL, Arbuckle K, et al. 2017. The biology of color. *Science*, **357**(6350): eaan0221.

David L, Rothbard S, Rubinstein I, et al. 2004. Aspects of red and black color inheritance in the Japanese ornamental (Koi) carp (*Cyprinus carpio* L.). *Aquaculture*, **233**(1-4): 129−147.

Du JX, Chen HL, Mandal BK, et al. 2021. HDL receptor/Scavenger receptor B1-*Scarb1* and *Scarb1-like* mediate the carotenoid-based red coloration in

fish. *Aquaculture*, **545**: 737208.
Elmadfa I, Majchrzak D. 1998. Carotenoids and vitamin A in fish. *Zeitschrift Fur Erziehungswissenschaft*, **37**(2): 207–210. (in German)
Eriksson J, Larson G, Gunnarsson U, et al. 2008. Identification of the *Yellow skin* gene reveals a hybrid origin of the domestic chicken. *PLoS Genetics*, **4**(2): e1000010.
Fujii R. 1993. Cytophysiology of fish chromatophores. *International Review of Cytology*, **143**: 191−255.
Fujii R. 2000. The regulation of motile activity in fish chromatophores. *Pigment Cell Research*, **13**(5): 300−319.
Garcia TI, Matos I, Shen YJ, et al. 2014. Novel method for analysis of allele specific expression in triploid *Oryzias latipes* reveals consistent pattern of allele exclusion. *PLoS One*, **9**(6): e100250.
Gazda MA, Araújo PM, Lopes RJ, et al. 2020. A genetic mechanism for sexual dichromatism in birds. *Science*, **368**(6496): 1270−1274.
Gillard GB, Grønvold L, Røsæg LL, et al. 2021. Comparative regulomics supports pervasive selection on gene dosage following whole genome duplication. *Genome Biology*, **22**(1): 103.
Granneman JG, Kimler VA, Zhang HM, et al. 2017. Lipid droplet biology and evolution illuminated by the characterization of a novel perilipin in teleost fish. *Elife*, **6**: e21771.
Gui JF, Zhou L. 2010. Genetic basis and breeding application of clonal diversity and dual reproduction modes in polyploid *Carassius auratus gibelio*. *Science China Life Sciences*, **53**(4): 409–415.
Hu FZ, Zhong HT, Fan JJ, et al. 2020. A new type of tetraploid fish derived via female autotetraploid × male allotetraploid hybridization. *Aquaculture*, **524**: 735244.
Huang X, Qin QB, Gong KJ, et al. 2020. Comparative analyses of the *Sox9a-Amh-Cyp19a1a* regulatory cascade in autotetraploid fish and its diploid parent. *BMC Genetics*, **21**(1): 35.
Hubbard JK, Uy JAC, Hauber ME, et al. 2010. Vertebrate pigmentation: from underlying genes to adaptive function. *Trends in Genetics*, **26**(5): 231−239.
Johnson AM, Fuller RC. 2015. The meaning of melanin, carotenoid, and pterin pigments in the bluefin killifish. *Lucania goodei. Behavioral Ecology*, **26**(1): 158−167.
Kiefer C, Sumser E, Wernet MF, et al. 2002. A class B scavenger receptor mediates the cellular uptake of carotenoids in *Drosophila*. *Proceedings of the National Academy of Sciences of the United States of America*, **99**(16): 10581–10586.
Kumar S, Stecher G, Tamura K. 2016. MEGA7: Molecular evolutionary genetics analysis version 7.0 for bigger datasets. *Molecular Biology and Evolution*, **33**(7): 1870−1874.
Lagarrigue S, Martin L, Hormozdiari F, et al. 2013. Analysis of allele-specific expression in mouse liver by RNA-Seq: a comparison with *Cis*-eQTL identified using genetic linkage. *Genetics*, **195**(3): 1157−1166.
Le Guyader S, Maier J, Jesuthasan S. 2005. *Esrom*, an ortholog of PAM (protein associated with c-*myc*), regulates pteridine synthesis in the zebrafish. *Developmental Biology*, **277**(2): 378−386.
Leclercq E, Taylor JF, Migaud H. 2010. Morphological skin colour changes in teleosts. *Fish and Fisheries*, **11**(2): 159−193.
Leggatt RA, Iwama GK. 2003. Occurrence of polyploidy in the fishes. *Reviews in Fish Biology and Fisheries*, **13**(3): 237−246.
Lehnert SJ, Christensen KA, Vandersteen WE, et al. 2019. Carotenoid pigmentation in salmon: variation in expression at *BCO2-l* locus controls a key fitness trait affecting red coloration. *Proceedings of the Royal Society B:Biological Sciences*, **286**(1913): 20191588.
Levy AA, Feldman M. 2004. Genetic and epigenetic reprogramming of the wheat genome upon allopolyploidization. *Biological Journal of the Linnean Society*, **82**(4): 607−613.
Li BJ, Chen L, Yan MZ, et al. 2023. Intercross population study reveals that co-mutation of *mitfa* genes in two subgenomes induces red skin color in common carp (*Cyprinus carpio wuyuanensis*). *Zoological Research*, **44**(2): 276−286.
Li BX, Vachali P, Frederick JM, et al. 2011. Identification of StARD3 as a lutein-binding protein in the macula of the primate retina. *Biochemistry*, **50**(13): 2541−2549.
Li WH, Liu JM, Tan H, et al. 2018. Asymmetric expression patterns reveal a strong maternal effect and dosage compensation in polyploid hybrid fish. *BMC Genomics*, **19**(1): 517.
Lin SM, Nieves-Puigdoller K, Brown AC, et al. 2010. Testing the carotenoid trade-off hypothesis in the polychromatic Midas cichlid. *Amphilophus citrinellus. Physiological and Biochemical Zoology*, **83**(2): 333−342.
Liu SY, Li YL, Wu Y, et al. 2012. Extraction, identification and quantitation of carotenoids in discolored channel catfish (*Ictalurus punctatus*) fillets. *Journal of Food Composition and Analysis*, **26**(1-2): 154−159.
Livak KJ. 2001. Analysis of relative gene expression data using real-time quantitative PCR and the 2(-Delta Delta C(T)) method. *Methods*, **25**(4): 402−408.
Lo HS, Wang ZN, Hu Y, et al. 2003. Allelic variation in gene expression is common in the human genome. *Genome Research*, **13**(8): 1855−1862.
Luo J, Chai J, Wen YL, et al. 2020. From asymmetrical to balanced genomic diversification during rediploidization: subgenomic evolution in allotetraploid fish. *Science Advances*, **6**(2): eaaz7677.
Martelotto LG, Ortiz JPA, Stein J, et al. 2007. Genome rearrangements derived from autopolyploidization in *Paspalum* sp. *Plant Science*, **172**(5): 970−977.
Mattingly KZ, Hovick SM. 2023. Autopolyploids of *Arabidopsis thaliana* are more phenotypically plastic than their diploid progenitors. *Annals of Botany*, **131**(1): 45−58.
Mecchia MA, Ochogavía A, Selva JP, et al. 2007. Genome polymorphisms and gene differential expression in a ‘back-and-forth’ ploidy-altered series of weeping lovegrass (*Eragrostis curvula*). *Journal of Plant Physiology*, **164**(8): 1051−1061.
Meléndez-Martínez AJ, Escudero-Gilete ML, Vicario IM, et al. 2010. Study of the influence of carotenoid structure and individual carotenoids in the qualitative and quantitative attributes of orange juice colour. *Food Research International*, **43**(5): 1289−1296.
Meyer A, Van De Peer Y. 2005. From 2R to 3R: evidence for a fish-specific genome duplication (FSGD). *Bioessays*, **27**(9): 937−945.
Ng'oma E, Groth M, Ripa R, et al. 2014. Transcriptome profiling of natural dichromatism in the annual fishes *Nothobranchius furzeri* and *Nothobranchius kadleci*. *BMC Genomics*, **15**(1): 754.
Ohkubo M, Tsushima M, Maoka T, et al. 1999. Carotenoids and their metabolism in the goldfish *Carassius auratus* (Hibuna). *Comparative Biochemistry and Physiology Part B:Biochemistry and Molecular Biology*, **124**(3): 333−340.
Parichy DM. 2003. Pigment patterns: fish in stripes and spots. *Current Biology*, **13**(24): R947−R950.
Plüddemann A, Neyen C, Gordon S. 2007. Macrophage scavenger receptors and host-derived ligands. *Methods*, **43**(3): 207−217.
Qin QB, Cao L, Wang YD, et al. 2019a. Rapid genomic and genetic changes in the first generation of autotetraploid lineages derived from distant hybridization of *Carassius auratus* red var. (♀) × *Megalobrama amblycephala* (♂). *Marine Biotechnology*, **21**(2): 139−149.
Qin QB, Liu QW, Wang CQ, et al. 2019b. Molecular organization and chromosomal localization analysis of 5S rDNA clusters in autotetraploids derived from *Carassius auratus* Red Var. (♀) × *Megalobrama amblycephala* (♂). *Frontiers in Genetics*, **10**: 437.
Qin QB, Wang YD, Wang J, et al. 2014. The autotetraploid fish derived from hybridization of *Carassius auratus red var*. (female) × *Megalobrama amblycephala* (male). *Biology of Reproduction*, **91**(4): 93.

Rashidian G, Rainis S, Prokić MD, et al. 2021. Effects of different levels of carotenoids and light sources on swordtail fish (*Xiphophorus helleri*) growth, survival rate and reproductive parameters. *Natural Product Research*, **35**(21): 3675−3686.

Ren L, Gao X, Cui JL, et al. 2022. Symmetric subgenomes and balanced homoeolog expression stabilize the establishment of allopolyploidy in cyprinid fish. *BMC Biology*, **20**(1): 200.

Ren L, Tang CC, Li WH, et al. 2017. Determination of dosage compensation and comparison of gene expression in a triploid hybrid fish. *BMC Genomics*, **18**(1): 38.

Shirak A, Shmarina A, Kuperman Y, et al. 2000. Inheritance of body and peritoneum color in hybrids of *Oreochromis aureus* and red *O. niloticus*. *Israeli Journal of Aquaculture Bamidgeh*, **52**(1): 21–29.

Soltis PS, Soltis DE. 2016. Ancient WGD events as drivers of key innovations in angiosperms. *Current Opinion in Plant Biology*, **30**: 159−165.

Song C, Liu SJ, Xiao J, et al. 2012a. Polyploid organisms. *Science China Life Sciences*, **55**(4): 301−311.

Song K, Lu P, Tang K, et al. 1995. Rapid genome change in synthetic polyploids of *Brassica* and its implications for polyploid evolution. *Proceedings of the National Academy of Sciences of the United States of America*, **92**(17): 7719−7723.

Song MJ, Potter BI, Doyle JJ, et al. 2020. Gene balance predicts transcriptional responses immediately following ploidy change in *Arabidopsis thaliana*. *The Plant Cell*, **32**(5): 1434–1448.

Song MY, Kim HE, Kim S, et al. 2012b. SNP-based large-scale identification of allele-specific gene expression in human B cells. *Gene*, **493**(2): 211−218.

Steffen JE, McGraw KJ. 2007. Contributions of pterin and carotenoid pigments to dewlap coloration in two anole species. *Comparative Biochemistry and Physiology Part B:Biochemistry and Molecular Biology*, **146**(1): 42−46.

Sundvold H, Helgeland H, Baranski M, et al. 2011. Characterisation of a novel paralog of scavenger receptor class B member I (*SCARB1*) in *Atlantic salmon* (Salmo salar). *BMC Genetics*, **12**(1): 52.

Toews DPL, Hofmeister NR, Taylor SA. 2017. The evolution and genetics of carotenoid processing in animals. *Trends in Genetics*, **33**(3): 171−182.

Toomey MB, Lopes RJ, Araújo PM, et al. 2017. High-density lipoprotein receptor *SCARB1* is required for carotenoid coloration in birds. *Proceedings of the National Academy of Sciences of the United States of America*, **114**(20): 5219−5224.

Van Bennekum A, Werder M, Thuahnai ST, et al. 2005. Class B scavenger receptor-mediated intestinal absorption of dietary β-carotene and cholesterol. *Biochemistry*, **44**(11): 4517−4525.

VanBuren R, Wai CM, Wang XW, et al. 2020. Exceptional subgenome stability and functional divergence in the allotetraploid *Ethiopian cereal* teff. *Nature Communications*, **11**(1): 884.

Van De Peer Y, Mizrachi E, Marchal K. 2017. The evolutionary significance of polyploidy. *Nature Reviews Genetics*, **18**(7): 411−424.

Veitia RA, Birchler JA. 2022. Gene-dosage issues: a recurrent theme in whole genome duplication events. *Trends in Genetics*, **38**(1): 1−3.

Von Lintig J, Moon J, Lee J, et al. 2020. Carotenoid metabolism at the intestinal barrier. *Biochimica et Biophysica Acta (BBA)-Molecular and Cell Biology of Lipids*, **1865**(11): 158580.

Wang CQ, Luo X, Qin H, et al. 2021a. Formation of autotriploid *Carassius auratus* and its fertility-related genes analysis. *BMC Genomics*, **22**(1): 435.

Wang CQ, Qin H, Zhao C, et al. 2021b. Whole-genome re-sequencing and transcriptome reveal oogenesis-related genes in autotetraploid *Carassius auratus*. *Marine Biotechnology*, **23**(2): 233–241.

Wang CQ, Zhou YW, Qin H, et al. 2020a. Genetic and epigenetic changes are rapid responses of the genome to the newly synthesized autotetraploid *Carassius auratus*. *Frontiers in Genetics*, **11**: 576260.

Wang S, Zhou P, Huang XX, et al. 2020b. The establishment of an autotetraploid fish lineage produced by female allotetraploid hybrids × male homodiploid hybrids derived from *Cyprinus carpio* (♀) × *Megalobrama amblycephala* (♂). *Aquaculture*, **515**: 734583.

Wang YD, Zhang MH, Qin QB, et al. 2019. Transcriptome profile analysis on ovarian tissues of autotetraploid fish and diploid red Crucian Carp. *Frontiers in Genetics*, **10**: 208.

Xu P, Xu J, Liu GJ, et al. 2019. The allotetraploid origin and asymmetrical genome evolution of the common carp *Cyprinus carpio*. *Nature Communications*, **10**(1): 4625.

Xu P, Zhang XF, Wang XM, et al. 2014. Genome sequence and genetic diversity of the common carp. *Cyprinus carpio*. *Nature Genetics*, **46**(11): 1212−1219.

Yang JH, Liu DY, Wang XW, et al. 2016. The genome sequence of allopolyploid *Brassica juncea* and analysis of differential homoeolog gene expression influencing selection. *Nature Genetics*, **48**(10): 1225−1232.

Yang Y, Wu LN, Chen JF, et al. 2020. Whole-genome sequencing of leopard coral grouper (*Plectropomus leopardus*) and exploration of regulation mechanism of skin color and adaptive evolution. *Zoological Research*, **41**(3): 328−340.

Yao H, Gray AD, Auger DL, et al. 2013. Genomic dosage effects on heterosis in triploid maize. *Proceedings of the National Academy of Sciences of the United States of America*, **110**(7): 2665−2669.

Yu P, Wang Y, Li Z, et al. 2022. Causal gene identification and desirable trait recreation in goldfish. *Science China Life Sciences*, **65**(12): 2341−2353.

Yu P, Wang Y, Yang WT, et al. 2021. Upregulation of the PPAR signaling pathway and accumulation of lipids are related to the morphological and structural transformation of the dragon-eye goldfish eye. *Science China Life Sciences*, **64**(7): 1031−1049.

Zhang TZ, Hu Y, Jiang WK, et al. 2015. Sequencing of allotetraploid cotton (*Gossypium hirsutum* L. acc. TM-1) provides a resource for fiber improvement. *Nature Biotechnology*, **33**(5): 531−537.

Zhang YQ, Liu JH, Peng LY, et al. 2017. Comparative transcriptome analysis of molecular mechanism underlying gray-to-red body color formation in red crucian carp (*Carassius auratus*, red var.). *Fish Physiology and Biochemistry*, **43**(5): 1387−1398.

Zhou L, Gui JF. 2017. Natural and artificial polyploids in aquaculture. *Aquaculture and Fisheries*, **2**(3): 103−111.

Zhou Y, Zhang XJ, Xu Q, et al. 2019. Nonadditive and allele-specific expression of insulin-like growth factor 1 in Nile tilapia (*Oreochromis niloticus*, ♀) × blue tilapia (*O. aureus*, ♂) hybrids. *Comparative Biochemistry and Physiology Part B:Biochemistry and Molecular Biology*, **232**: 93−100.

Zhu FJ, Schlupp I, Tiedemann R. 2017. Allele-specific expression at the androgen receptor alpha gene in a hybrid unisexual fish, the Amazon molly (*Poecilia formosa*). *PLoS One*, **12**(10): e0186411.

Zhuo Z, Lamont SJ, Abasht B. 2017. RNA-Seq analyses identify frequent allele specific expression and no evidence of genomic imprinting in specific embryonic tissues of chicken. *Scientific Reports*, **7**(1): 11944.